8-2003

A Design Study of a Proposed Four-Seat, Amateur-Built Airplane

D. Andrew Moore
University of Tennessee - Knoxville

To the Graduate Council:

I am submitting herewith a thesis written by D. Andrew Moore entitled "A Design Study of a Proposed Four-Seat, Amateur-Built Airplane." I have examined the final electronic copy of this thesis for form and content and recommend that it be accepted in partial fulfillment of the requirements for the degree of Master of Science, with a major in Mechanical Engineering.

Dr. Gary Flandro, Major Professor

We have read this thesis and recommend its acceptance:

Dr. Louis Deken, Dr. Peter Solies

Accepted for the Council:
Carolyn R. Hodges

Vice Provost and Dean of the Graduate School

(Original signatures are on file with official student records.)

To the Graduate Council:

I am submitting herewith a thesis written by D. Andrew Moore entitled “A Design Study of a Proposed Four-Seat, Amateur-Built Airplane.” I have examined the final electronic copy of this thesis for form and content and recommend that it be accepted in partial fulfillment of the requirements for the degree of Master of Science, with a major in Mechanical Engineering.

Dr. Gary Flandro
Major Professor

We have read this thesis
and recommend its acceptance:

Dr. Louis Deken

Dr. Peter Solies

Accepted for the Council:

Dr. Anne Mayhew
Vice Provost and Dean of Graduate Studies

(Original signatures are on file with official student records.)

A DESIGN STUDY OF A PROPOSED FOUR-SEAT, AMATEUR-BUILT AIRPLANE

A Thesis

Presented for the

Master of Science

Degree

The University of Tennessee, Knoxville

D. Andrew Moore

August 2003

Dedicated to

my Father

who enabled me to fly

and to

Michael Reisman

who showed me how.

Acknowledgments

The author wishes to express special appreciation to Dr. Gary Flandro, fellow sailplane enthusiast, advisor and head of my thesis committee, for allowing me the flexibility to pursue the design project herein. His patience with my many distractions balanced with his persistent encouragement were essential to the successful completion of this project.

The author is additionally grateful to Dr. Lou Deken, thesis committee member and professor who taught many of the courses that provided the cornerstone for the work presented herein.

Recognition and thanks go to Dr. Peter Solies for his valuable insights while participating on this thesis committee and especially for his unwavering dedication to the University soaring club all of these years.

The author will be forever indebted to his wife Suzanne for providing inspiration by example and always believing in the successful completion of this project.

Abstract

An airplane configuration suitable for construction by an amateur builder without the need for complex factory fixtures and tooling has been developed. The proposed high-wing configuration is intended to carry a 600 LB payload of up to 4 passengers arranged in 2 rows of side-by-side accommodations at a design cruise speed of 145 kts.

It has been shown that the cantilevered wing components of the low-wing, 2-seat Mustang II kit airplane are ideally suited for the proposed airplane when properly matched with strut braced inboard wing panels. The structural implications of optimally sized ailerons on the baseline Mustang II wing structure is presented. Wing, fuselage, and strut reaction loads have been determined for the proposed flight envelope. A steel tube cabin structure has been proposed and limited structural optimization accomplished using a finite-element model. Detail analysis of the wing/fuselage, wing/strut and strut/fuselage attachment fittings has been accomplished.

TABLE OF CONTENTS

CHAPTER PAGE

1. INTRODUCTION....1

2. CONFIGURATION DEVELOPMENT....3

2.1 Mission....3
2.2 Configuration....3
2.3 Construction....4
2.4 Engine/Propellor....5
2.5 Initial Sizing....5
2.6 Center of Gravity Variation and Wing Placement....9
2.7 Empennage Sizing and Placement....12
2.8 Aileron Sizing....13
2.9 Landing Gear Arrangement....14
2.10 Composite Configuration Layout....15

3. FLIGHT ENVELOPE....18

3.1 Performance Estimate....18
3.2 Structural Flight Envelope....22

4. WING LOADS....28

4.1 Average Loads....28
4.2 Span-wise Load Distribution....30
4.3 Outer Panel Loads....30
4.4 Total Wing Attachment Reaction Loads....38

5. WING STRUCTURE....43

5.1 General....43
5.2 Outboard Wing Panel Attachments....43
5.3 Inboard Wing Panel Main Spar....45
5.4 Wing/Strut Attachment....49
5.5 Forward Wing/Fuselage Attachment....50
5.6 Aft Wing/Fuselage Attachment....51

6. FUSELAGE STRUCTURE....54

6.1 Steel Cabin Frame....54
6.2 Special Consideration to Lateral Reactions....58
6.3 Fuselage Attachment Fittings....60

CHAPTER PAGE

6.4 Wing Strut.....63

7. CONCLUSIONS AND RECOMMENDATIONS.....67

7.1 Conclusions.....67
7.2 Recommendations.....67

REFERENCES AND BIBLIOGRAPHY.....68

VITA.....71

LIST OF TABLES

TABLE PAGE

1. Wing Loading Comparison of Certified Aircraft....8
2. Payload Effect on Center of Gravity....12
3. Tail Volume Comparison....13
4. Airfoil Characteristics....22
5. Airplane Categories and Design Load factors....22
6. Gust Load Factors....26
7. Average Wing Aerodynamic Coefficients....30
8. Outer Wing Panel Aileron-Deflected Torsion Estimate....36
9. Outer Wing Panel Reaction Load Components....38
10. Outer Wing Panel Combined Reaction Loads....39
11. Wing Reaction Load Components....41
12. Wing Combined Reaction Loads....42
13. Material Mechanical Properties....43
14. Finite Element Model Applied Loads....56
15. Critical Fuselage Tube Properties....59
16. Summary of Fuselage Fitting Stresses....64

LIST OF FIGURES

FIGURE PAGE

1. Wing Planform Comparison....7
2. Mean Aerodynamic Chord (mac)....9
3. Allowable CG Variation....10
4. Fuel Tank Center of Gravity....11
5. Suggested Aileron Size....14
6. Landing Gear Placement....15
7. Composite Configuration Layout....16
8. Proposed Planform Comparison with Cessna 170B Wing....21
9. Load Factor Variation with Weight (W/S = 83.51 lb/ft^2)....23
10. Sample V-n Diagram....24
11. Proposed Structural Flight Envelope....27
12. Force Coefficient Variation with Angle of Attack....29
13. Span-wise Distribution of Normalized Lift and Drag Coefficients....31
14. Span-wise Unit Coefficient Distribution....31
15. Wing Outer Panel Shear Force Distribution....33
16. Wing Outer Panel Bending Moment Distribution....33
17. Wing Outer Panel Bending Stress Distribution....34
18. Mustang II Aft Spar Attachment Fitting....44
19. Inboard Wing Panel, Main Spar Details....46
20. Inboard Wing Panel, Shear and Moment Diagram....47
21. Inboard Wing Panel, Span-wise Normal Stress Distribution....47

FIGURE PAGE

22. Inboard Wing Panel, Aft Spar Attachment Fitting Rivet Loads.....52

23. Cabin Steel Tubing Arrangement.....55

24. Finite Element Model.....55

25. Tubing Axial Loads.....57

26. Tubing Moments.....57

27. Combined Axial and Bending Normal Stress.....59

28. Fuselage Attachment Fitting, Strut and Main Wing Spar.....61

29. Fuselage Attachment Fitting, Aft Wing Spar.....61

30. Fitting Weld Approximation.....64

31. Streamlined Strut Cross Section.....65

32. Strut End Fitting.....65

NOMENCLATURE

a	Lift curve slope
A	Aspect ratio (b^2 / S)
A_{bolt}	Fastener cross section area
b	Wing span
b_o	Outboard wing panel span
c	Wing chord
$\bar{c}$	Mean aerodynamic chord (mac)
C_A	Axial-force coefficient
cg	Center of gravity
C_L	Lift coefficient
C_{L_α}	Lift curve slope
C_m	Moment coefficient
C_N	Normal-force coefficient
c_{v_h}	Horizontal tail volume coefficient
d	Fastener diameter
D	Drag force
e	Wing efficiency factor (0.8 for high wing)
E	Material modulus of elasticity
g	Acceleration due to gravity
h	Spar depth

h'	Effective spar depth between the flange centroids
K_g	Gust reduction factor
$K_{fitting}$	Additional safety factor applied to the fitting design
K_s	Shear web diagonal tension factor
L	Lift force
l_t	Distance from the wing mac to the horizontal tail mac
M	Wing moment
mac	Mean aerodynamic chord
n	Load factor (g's)
n_1	Maximum allowable positive load factor (g's)
n_3	Maximum allowable negative load factor (g's)
q	Dynamic pressure
R	Reaction force
S	Wing area
S_h	Horizontal tail area
t	Material thickness
T	Wing torsion
U_{de}	Derived gust velocity
V	Airplane equivalent speed or shear force
V_A	Airplane maneuvering speed
V_C	Airplane cruise speed
V_D	Airplane dive speed
V_S	Stall speed

W	Weight
$w_{fuselage}$	Fuselage width
X	Fuselage station measured aft from the firewall
y	Span station
α	Angle of attack
$\alpha_{C_{L0}}$	Angle of attack for zero lift coefficient
δ_b	Allowable aileron deflection at the maximum dive speed
δ_{15}	Maximum aileron deflection (15 deg, trailing edge down)
Δ_p	Total aileron travel
ΔX_{spars}	Distance between the forward and aft wing spars
Δy_{strut} Vertical distance	between the fuselage/strut attachment and the forward fuselage/wing spar attachment
Δz_{strut}	Lateral distance between the wing/strut attachment and the forward fuselage/wing spar attachment
ρ	Air density
σ	Normal stress
σ_b	Bearing stress
σ_{bu}	Material ultimate bearing strength
σ_d	Material design strength
σ_{tu}	Material ultimate tensile strength
σ_{ty}	Material yield tensile strength
τ	Shear stress

τ_d	Material design shear strength
τ_u	Material ultimate shear strength
μ_g	Airplane mass ratio

Subscripts:

ac	Aerodynamic center
aft	Aft spar
axial	Relating to axial stress
bending	Relating to bending stress
cp	Center of pressure
C170	Cessna 170
C180	Cessna 180
c / 4	With respect to the 25% chord location
down	Trailing edge down
fwd	Forward (main) spar
i	Subscript (aft, fwd, strut)
up	Trailing edge up
web	Shear web

1. INTRODUCTION

For an aircraft to qualify as "amateur-built" in accordance with the Federal Aviation Administration (FAA) regulations, at least 51% of its construction must be accomplished by the owner [1]. Amateur-built aircraft are completed from plans and raw materials or from kits that include component sub-assemblies of varying degrees of completion. With only a few exceptions, qualified amateur-built aircraft designs are powered by a single engine.

The huge number of amateur-built aircraft that attend the popular Experimental Aircraft Association (EAA) flying at Oshkosh, WI demonstrates the growing interest in this type of aircraft ownership. There are a number of factors that motivate an amateur aircraft builder to invest the many hundreds, sometimes thousands of hours required to bring their projects to completion. Because designers of amateur-built aircraft designs are not burdened with the expensive and time consuming process of FAA certification, they can more easily take advantage of new technologies that can provide significant performance and even safety improvements. The construction costs associated with an amateur-built are generally less than half, sometimes much less than half, than the cost of comparable new factory-built aircraft. At comparable cost, the factory-built alternatives will generally be in the form of aging, vintage aircraft, which have their own appeal to many enthusiasts, but which are generally of low to moderate performance. Additionally, the amateur airplane builder is allowed to accomplish all necessary maintenance, including required annual inspections, that can easily exceed $1000 for some vintage factory-built

airplanes.

The purpose of the study presented herein is to develop an aircraft design that is well suited to methods of construction generally employed by amateur aircraft builders and not requiring a significant investment in jigging or tooling. The author has found it necessary to pursue a new airplane design in order to control the inevitable design compromises and achieve specific design goals.

2. CONFIGURATION DEVELOPMENT

2.1 Mission

The primary mission of the proposed airplane is to provide accommodations for two full-sized adults during sport flying, including scenic touring, basic acrobatics, and occasional travel. A nominally 600 lb payload (not including fuel) will allow plenty of optional baggage, or an extra passenger or two, depending on size. A no-reserve endurance of 4 hours at a cruise speed not less than 140 kts will provide reasonable travel capability. Although not intended for operation from rough, back-country airstrips, operation from private grass runways is considered necessary in light of the alarming rate at which general aviation runways are being closed (there are 25% fewer public use airports today than in 1969 [2]). Therefore, the installed engine/propeller performance must be sufficient to allow comfortable operation from relatively short (2500 ft), unpaved airfields possibly obstructed by trees and/or power lines.

2.2 Configuration

Passenger and/or baggage accommodations will be provided in two rows of seats with passenger cabin access on both left and right sides. No separate baggage area is planned. The proposed cabin is generally based on a 2-inch-wider version of the Cessna 170B cabin, which has proved by experience to be very suitable in practice. The resulting cabin dimensions are 42” wide, 43” tall, and 90” long. The proposed airplane design will utilize a high-wing

configuration. In comparison with low-wing configurations, the high-wing configuration offers a number of practical advantages including simple gravity flow fuel systems, unrestricted visibility to the ground, simplified egress (good for passengers with mobility limitations, especially after an accident), and cabin shade from both the sun and rain (especially nice when loading and/or unloading during inclement weather). In addition to the practical advantages stated, the high-wing configuration also has an aerodynamic efficiency advantage over the low-wing configuration [3].

The proposed configuration will employ a conventional, aft mounted horizontal and vertical tail for stability and control. A conventional, tailwheel landing gear configuration will be used, because it is considered better suited than the tricycle configuration for operating from private airstrips, which sometimes require taxi operations in confined spaces and takeoff from relative rough and uneven runways. The main landing gear will utilize a simple, low-maintenance, non-retractable installation. No discussion about landing gear design will be presented herein.

The proposed configuration is inspired by the Cessna 170 and 180, 4-seat, tailwheel airplanes in which the author has considerable experience. The primary difference will be size, as the proposed airplane will be smaller and more optimized for 2 passengers.

2.3 Construction

Since the proposed design will likely be a one-of-a-kind and not intended for high-rate production, its construction must be possible without a significant

investment in single-use jigging or tooling. Where possible, components from existing airplanes will be utilized. The primary cabin structure will be made from steel tubing. Steel tubing was selected for use in the cabin area, because it is easy to analyze, especially when using computer methods, is easy to assemble, and is easy to repair when damaged. The horizontal and vertical tails will be aluminum cantilever structures, and the tail cone will use semi-monocoque construction of aluminum.

2.4 Engine/Propeller

Sport aviation aircraft are generally designed around a relatively small selection of suitable aircraft engines. An even smaller group of engine candidates use low enough compression to allow operation on less expensive and more available automotive fuel. The planned use of automotive fuel limits the baseline engine for the proposed airplane to a low compression engine of nominally 230 HP represented by either a 470 cu-in Continental or 540 cu-in Lycoming. Consistent with existing certified airplanes using the same engine type, the baseline propellor will be length-limited to 82 inches. Fuel consumption of the 230 hp engine during a leaned, cruise condition at 75% maximum power is about 12 gal/hr. Given the 4 hr endurance requirement, a useful fuel capacity of at least 48 gallons is required.

2.5 Initial Sizing

Initial aircraft sizing involves the optimization of the wing geometry for given aircraft weight and mission. The classical design process optimizes the wing geometry according to weighted requirements for each phase of the flight

mission including takeoff, climb, cruise, maneuvering, and landing. Unlike a classical design-from-scratch process, the proposed airplane has been designed around a wing that can be built, in part, using existing components.

The idea for the proposed airplane came about after studying the wing of the Mustang II kit airplane [4]. The Mustang II is a high-performance 2-seat design, currently marketed by Mustang Aeronautics, that evolved from the single seat Long Midget racer (Midget Mustang) designed and built in 1948 by Dave Long, chief engineer at Piper Aircraft. Credit to the Mustang II design belongs to Robert Bushby who started building the prototype in 1963 after obtaining the design rights to the Midget Mustang in 1959. Figure 1 shows how the Mustang II 3-piece wing evolved from the Midget Mustang wing by adding a constant chord center section. The Mustang II wing is built in 3 pieces, and the 2 outboard portions easily detach from the center section. A logical extrapolation from the 3-piece wing is a 4-piece wing of greater span and area which can accommodate heavier payloads including extra passenger(s). This observation is the foundation for the proposed airplane.

The proposed wing is shown to have a span of 33 ft span and a corresponding area of 141 sq-ft. The span/area combination was selected after estimating a gross weight of 2400 lbs and selecting a design wing loading of 17 lb/ft^2. The gross weight estimate was based on an estimated empty weight of 1500 lb (about like a Cessna 180 [5]) and a 900 lb payload, including the minimum fuel weight of nominally 300 lb (50 gals). The wing loading selection was based on the data in Table 1.

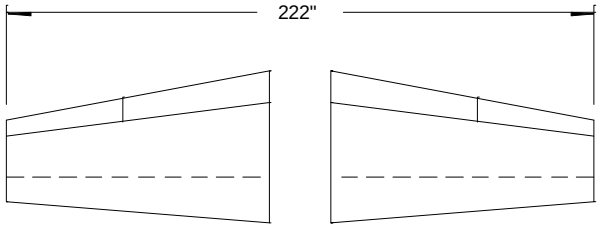

Midget Mustang planform

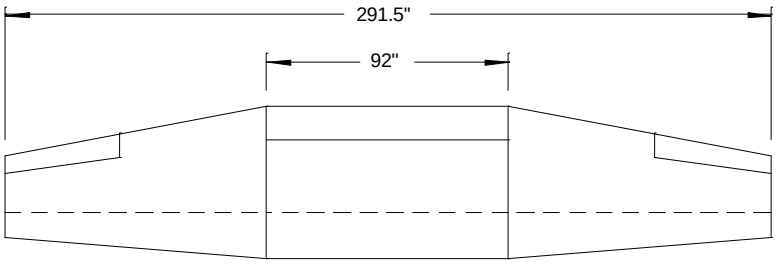

Mustang II, 3-piece planform

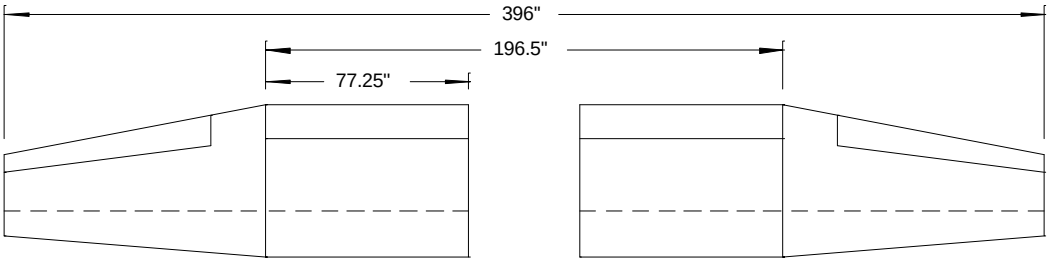

Proposed, 4-piece, strut-braced, high wing planform

Figure 1. Wing Planform Comparison.

Table 1. Wing Loading Comparison of Certified Aircraft [5].

Model	W (lbs)	S (ft2)	W/S (lb/ft2)
Stinson 108	2400	155.0	15.5
Beech C33	3050	177.0	17.2
Money M-20F	2740	167.0	16.4
Maule M-5-235	2450	157.9	15.5
Cessna 170B	2200	175.0	12.6
Cessna 182D	2950	174.0	17.0
Cessna 185	3350	174.0	19.3
Piper PA-24-260	3200	178.0	18.0
Piper PA-28-200R	2650	170.0	15.6
Piper PA-28-235D	3000	171.0	17.5
Commander 114B	3250	152.0	21.4

The two inboard panels will attach to the top of the steel cabin structure and be strut braced. Strut bracing the inboard panels will effectively limit the maximum wing bending moments to the values experienced at the attachment point of the outer wing panels. The mean aerodynamic chord (mac) length for the proposed wing is 52.7 inches according to:

$$\bar{c} = \frac{1}{S}\int_{-b/2}^{b/2} c^2 \, dy$$

The outer wing panel chordwise taper is coincident with the main spar and nominally 30% aft of the wing leading edge. With common 30% chord locations, the leading edge of the mac is 1.6 inches aft of the root leading edge as shown in Figure 2.

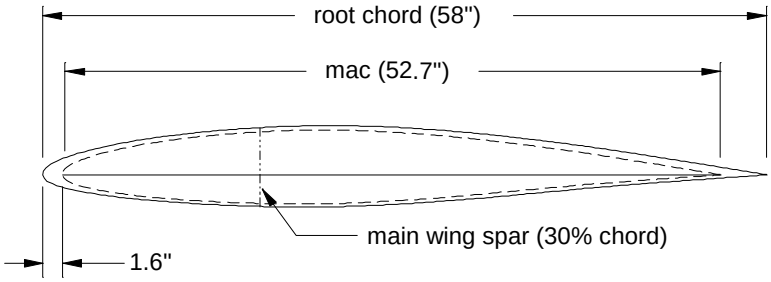

Figure 2. Mean Aerodynamic Chord (mac).

2.6 Center of Gravity Variation and Wing Placement

The allowable center of gravity (cg) range of the proposed airplane will depend on both the its stability and controllability. The forward aircraft cg limit is generally established by controllability limitations during the flare to landing, while the aft limit is established by minimum acceptable stability. Analytical methods for estimating airplane stability and controllability involve as-yet undetermined lift characteristics for both the wing and the horizontal tail as well as the relative size and placement of the horizontal tail. Comparing the cg range for existing airplanes can provide an expectation for acceptable variation. Figure 3 shows the center of gravity ranges for a number of aircraft, both certified and experimental.

Even without knowing the acceptable cg limits, it is possible to estimate the cg variation associated with the disposable payload (passengers, baggage, and fuel). For the proposed airplane, the main fuel tanks will be contained in the leading edges of the 2 inboard wing panels using construction methods similar to those employed in the popular RV series of kit airplane [6]. Given the span of

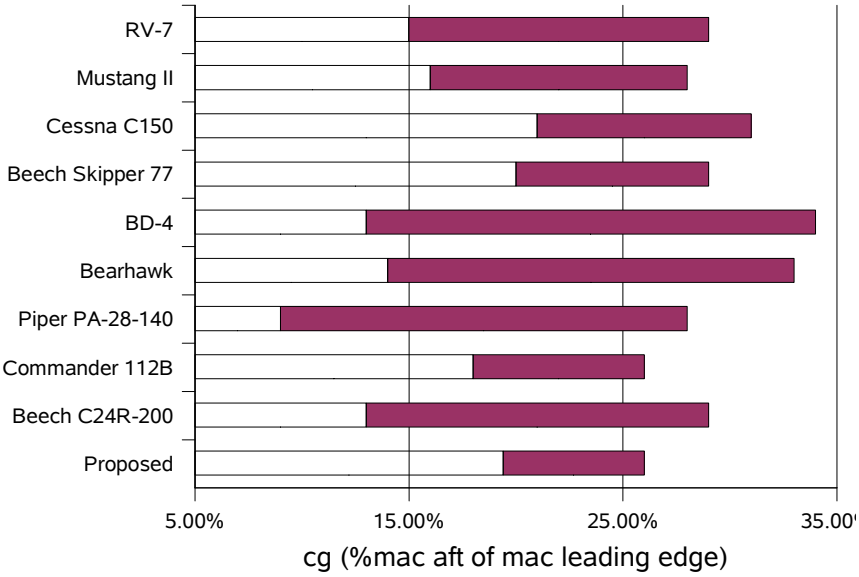

Figure 3. Allowable CG Variation.

the inboard panels and the airfoil geometry ahead of the wing main spar, the maximum possible fuel volume will be approximately 50 gallons with a full-tank cg 9.6 inches aft of the root chord leading edge (Figure 4). The location of the front and rear seats of the proposed airplane will be the same as in the Cessna 170B, so the passenger cg will be located at stations 36 and 70 (inches aft of the firewall) for the front and rear seat passengers, respectively.

Some estimate for the wing position is necessary in order to consider the effect of the fuel weight. Fortunately, the cg variation associated with changes in payload proved not to be especially sensitive to the wing position. Of greater importance to acceptable cg travel is the empty cg. For a given wing position, there exists an optimum empty cg that will minimize the cg variation for the possible payload states. Once determined, an optimum empty cg location can

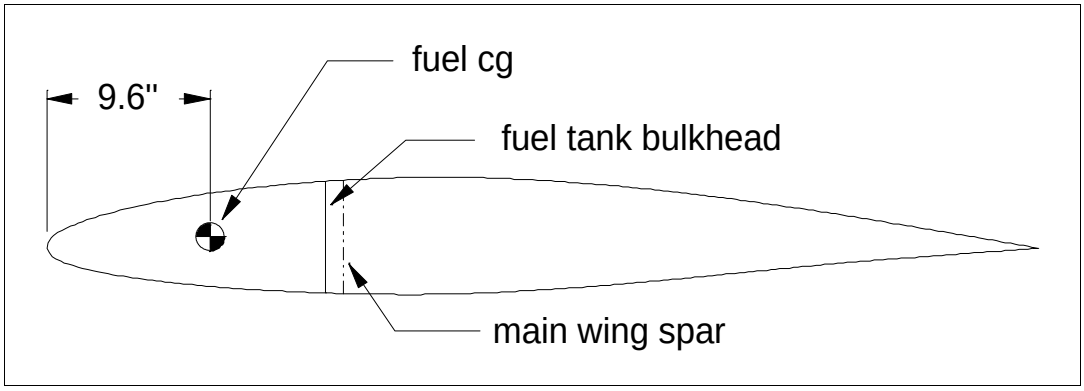

Figure 4. Fuel Tank Center of Gravity.

generally be achieved during construction with judicious placement of the battery. In more extreme cases, the engine may need to move forward or backward.

For the proposed airplane, the location of the wing aerodynamic center (25% of the mac) with respect to the firewall reference was determined according to:

$$X_{ac} = X_{ac_{C170}} \sqrt{\frac{S}{S_{C170}}} = 35.6\,inches$$

The leading edge station of the root chord can then be determined by:

$$X_{LE} = X_{ac} - 0.25 \cdot mac + 1.9\,inches = 20.82\,inches$$

Table 2 shows the resulting payload effect on the cg variation for a number of loading scenarios. The cg calculations were based on an empty cg coincident with 20% mac. For comparison, the resulting cg variation is also shown in Figure 3.

Table 2. Payload Effect on Center of Gravity.

Fuel (gal)	0	0	50	50	50
Front Seat (lbs)	0	100	100	400	400
Rear Seat (lbs)	0	0	0	0	200
Gross Weight (lbs)	1500	1600	1900	2200	2400
cg (STA)	33.0	33.1	32.7	33.2	36.2
cg (%mac)	20.0%	20.4%	19.5%	20.4%	26.2%

2.7 Empennage Sizing and Placement

The moment created by the tail is necessary for aircraft trim, control and stability. The tail moment is proportional to the product of the tail area and the distance of the tail from the airplane cg, and the tail volume coefficient provides a convenient way to describe the relative effectiveness of the tail at producing moments. The horizontal tail volume coefficient is defined as:

$$c_{v_h} = \left(\frac{S_{tail}}{S}\right)\left(\frac{l_{tail}}{\bar{c}}\right)$$

Appropriate tail sizing and placement is critical to obtaining the desired stability and control characteristics. For any given airplane cg, an increase in tail volume coefficient adds stability but decreases maneuverability, while a decrease in tail volume improves maneuverability but relaxes the stability. In order to establish a reasonable target tail volume coefficient, a survey of existing airplanes is useful. Table 3 shows the tail volume coefficient data for a number of representative airplanes. In all cases the tail lengths represent the distance between the wing aerodynamic center (25% mac) and the tail

Table 3. Tail Volume Comparison.

Airplane	S_h / S	l_t / mac	c_{v_h}
RV-10	0.23	2.75	0.63
RV-9	0.22	2.35	0.54
RV-7	0.19	2.26	0.43
BD-4	0.21	3.0	0.63
Cessna 170B	0.20	2.97	0.59
Bearhawk	0.19	2.27	0.43
Mustang II	0.17	2.5	0.43
Proposed	0.19	2.7	0.53

aerodynamic center (25% mac of the tail).

The desire to utilize components from existing airplanes resulted in the decision to adapt the RV-9 tail to the proposed design. Even though the wing areas are different, Table 3 shows that proper location of the tail results in essentially the same tail volume falling between the values for the Mustang II and the Cessna 170B

2.8 Aileron Sizing

The ailerons for the proposed wing will have the same chord fraction (22.4%) as the Mustang II ailerons but will be of increased span (and area) by moving the aileron root rib more inboard. An estimate for the required aileron span was based on design limits shown in Figure 5. Accordingly, an aileron span of 0.37% of the semi-span was selected.

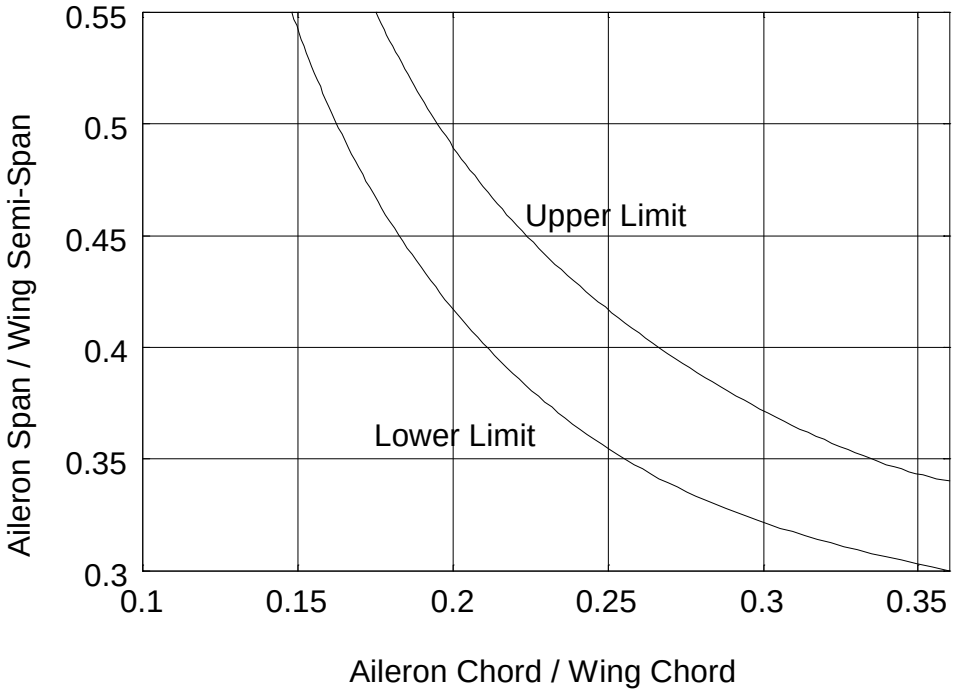

Figure 5. Suggested Aileron Size [7].

2.9 Landing Gear Arrangement

Considerations for optimizing the conventional (tail wheel) landing gear arrangement included 1) a 3-point wing incidence of 12-15 degrees while still allowing good over-the-nose field of view while taxiing [8], 2) a 9-inch minimum propeller clearance at takeoff in accordance with FAR Part 23 [9], and 3) reasonable resistance to tip-over during braking upon landing while also limiting the tail wheel loads. Criteria 1) and 2) affect the landing gear length, while criteria 3) affects the axial placement of the wheel with respect to the cg. From the landing gear design perspective, the cg includes both axial and vertical dimensions. For the discussion herein, the vertical cg is considered coincident

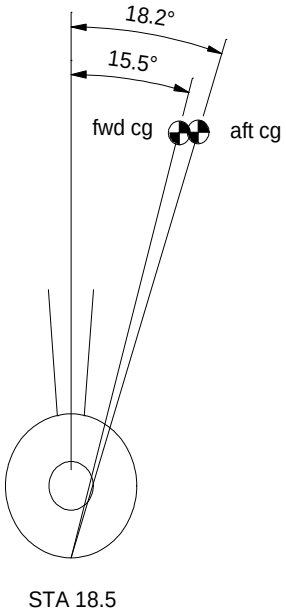

Figure 6. Landing Gear Placement.

with the propellor centerline. The axial cg variation was shown previously in Figure 3. The primary design parameter is the relative angle between a vertical line and a line passing through the wheel/ground contact point and the cg. Satisfactory landing gear design generally requires this angle to fall within the range from 15-25 deg. Figure 6 shows an acceptable variation for the predicted cg variation with the wheel located 18.5 inches aft of the firewall.

2.10 Composite Configuration Layout

Given the proposed wing, cabin, tail and landing gear configurations, the composite configuration, shown in Figure 7, was established. Note that the proposed configuration has, by design, significant similarity with the Cessna 170/180 aircraft. One interesting observation is that of the major sub-components (outboard wing, inboard wing, cabin, tail cone and tail surfaces)

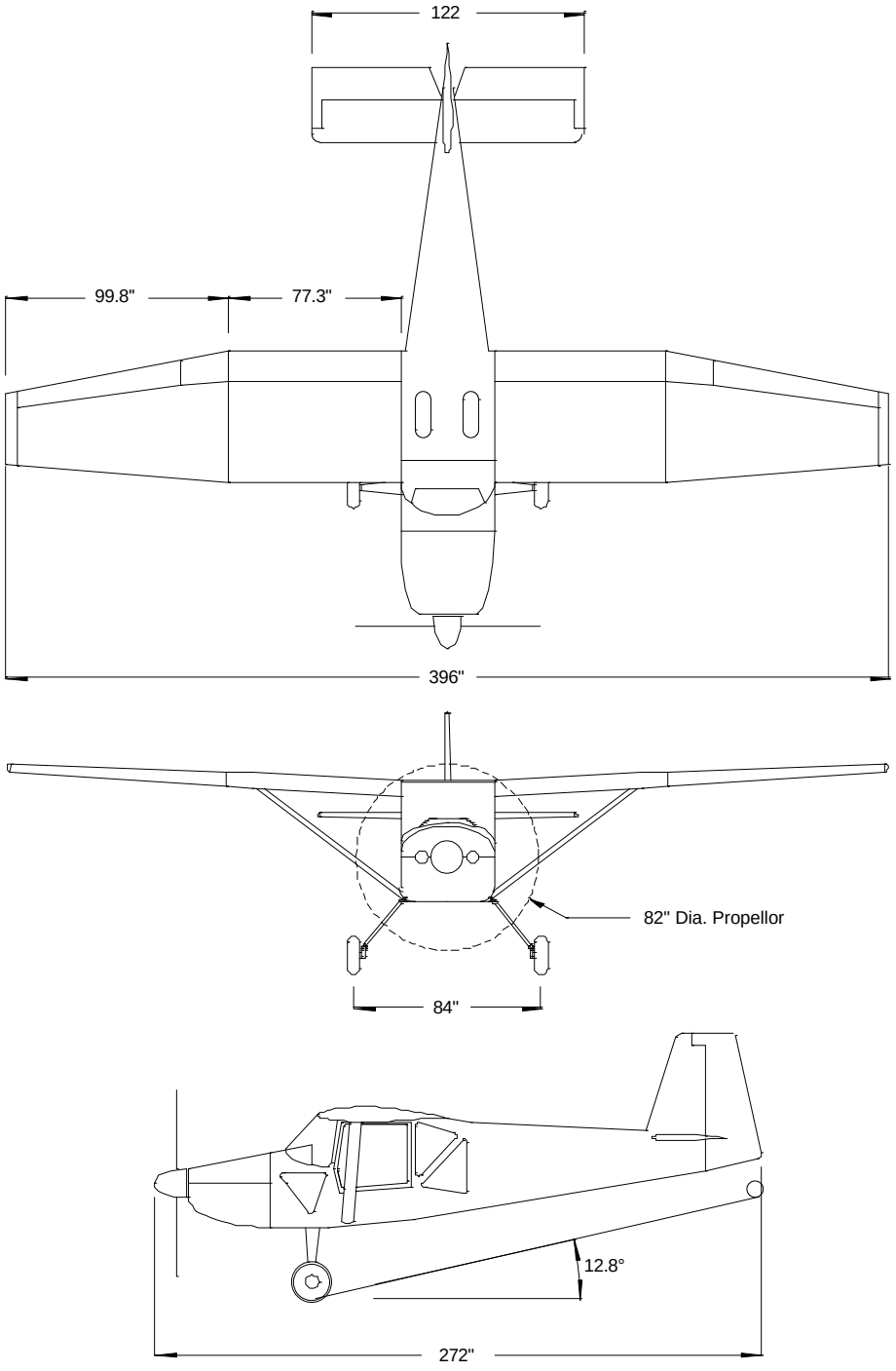

Figure 7. Composite Configuration Layout.

the horizontal tail is the largest at nominally 10 ft, making it possible to build all of the major sub-components in a relatively small workshop.

3. Flight Envelope

3.1 Performance Estimate

From the pilot's perspective, the two most important airplane performance parameters are the cruise and stall speeds. Establishing target values for both the cruise and stall speeds is often the first design decision and requires an optimization process to achieve the correct weighted balance of best cruise and stall speeds. A relatively low stall speed allows a relatively slow landing approach which is easier and safer to accomplish. Unfortunately, the relatively lower wing loading (i.e. relatively larger wing area) required to achieve relatively lower stall speeds decreases the cruise speed for any given engine/propellor installation. Since good cruise speed is what sells most airplane designs, the cruise speed is frequently weighted more heavily than stall speed during the optimization, but the FAA does limit maximum allowable stall speeds for certified single engine aircraft to 61 kts [9].

Although target performance speeds were not explicitly optimized for the proposed airplane design, the configuration-development decision process certainly included implicit expectations with respect to performance. Because of the configuration and proportion similarities, the cruise performance of the proposed airplane may be estimated with respect to the known cruise performance of the Cessna 180 that also uses a 230 HP engine. By assuming that the proposed airplane has, by similarity, the same non-dimensional drag coefficient as the Cessna 180, then for similar engine/propellor installations, the

cruise speeds will be proportional to the cubed root of the wing area ratio. Given the Cessna 180 cruise speed of 140 kts [5], the estimated cruise speed for the proposed airplane will be:

$$V_C = V_{C_{C180}} \sqrt[3]{\frac{S_{C180}}{S}} = 150\,\text{kts}$$

The NACA 64212 airfoil section employed on the proposed wing is optimized for drag at a wing section lift coefficient of 0.2 (± 0.1) [10]. An estimate of the cruise wing lift coefficient will validate the applicability of the proposed wing to the expected 150 kts cruise condition. Starting with the basic lift equation:

$$L = W = \frac{1}{2}\rho V^2 S C_L$$

the lift coefficient is:

$$C_L = \frac{2W}{\rho S V^2} \qquad 3.1$$

and associated velocity is:

$$V = \sqrt{\frac{2W}{\rho S C_L}} \qquad 3.2$$

At a cruise speed of 150 kts, the total airplane trim lift coefficient can be determined from Equation 3.1 to be 0.22. The total airplane lift includes contributions from both the wing and tail:

$$L = L_{wing} + L_{tail}$$

where the tail lift must balance the moments about the cg to achieve a trimmed state. If the cg is considered coincident with the aerodynamic center, then:

$$L_{tail} = \frac{M_{ac}}{l_t}$$

therefore:

$$L_{wing} = L - \frac{M_{ac}}{l_t}$$

or in coefficient form:

$$C_{L_{wing}} = C_L - C_m \frac{\bar{c}}{l_t} \qquad 3.3$$

Making the proper substitutions into Equation 3.3 results in a wing lift coefficient of 0.23 at the cruise condition, which is well within the optimum drag bucket of the NACA 64212 airfoil and implies that the proposed wing should be reasonably well optimized.

Although the proposed design does not have to comply with FAA guidelines on maximum allowable stall speed, a stall speed estimate for the proposed airplane and comparison with the guideline provides additional validation of selected wing size. The stall speed is the minimum speed for which a steady flight path can be achieved and occurs at the maximum total trim lift coefficient. The total maximum lift coefficient is estimated according to:

$$C_{L_{max}} = C_{L_{max_{wing}}} + C_m \frac{\bar{c}}{l_t}$$

Note that moment coefficient is generally negative for non-symmetric wing airfoils, so the tail contribution necessary for trim decreases the maximum total lift coefficient. A number of independent parameters affect the maximum wing lift coefficient including the maximum airfoil section lift coefficient, the wing

aspect ratio and spanwise twist characteristics. Because of the overall configuration similarities and especially the similarities of the wing planforms shown in Figure 8, an empirical estimate for the total maximum lift coefficient of the proposed airplane will be made based on the known performance of the Cessna 170B.

Cessna 170B has a 50 kts flaps-retracted stall speed established during certification flight testing [11]. Using the wing loading properties shown in Table 1, the maximum total airplane lift coefficient for the Cessna 170B can be determined to be:

$$C_{L_{max_{C170}}} = \frac{2W}{\rho S_{C170}(V_{S_{C170}})^2} = 1.485$$

One difference, relevant to lift coefficient, between the Cessna 170B and the proposed airplane is the difference in the wing airfoil section coefficients shown in Table 4. If maximum airfoil section lift coefficient is assumed to have the greatest effect on maximum wing lift coefficient and the wing is assumed to contribute most of the total airplane lift, then a first-order estimate of the proposed airplane lift coefficient can be made as:

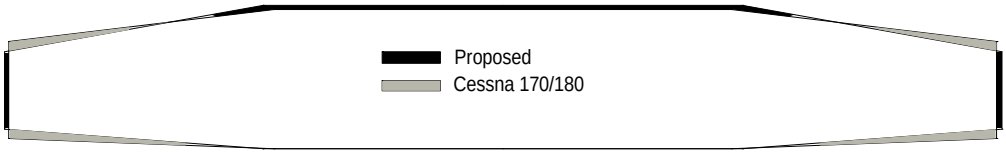

Figure 8. Proposed Planform Comparison with Cessna 170B Wing [11].

Table 4. Airfoil Characteristics [10].

Airplane	Airfoil	$C_{l_{max}}$	$C_{m_{mac}}$
Cessna 170B	NACA 2412	1.6	-0.045
Proposed	NACA 64_1-212	1.55	-0.025

Table 5. Airplane Categories and Design Load Factors [9].

Category	Load Factor, n_1 (g's)
Standard	3.8
Utility	4.4
Acrobatic	6

$$C_{L_{max}} = C_{L_{max_{C170}}} \frac{C_{l_{max_{NACA64212}}}}{C_{l_{max_{NACA2412}}}} = 1.439$$

Substituting the estimated maximum lift coefficient into Equation 3.2 results in a flaps-retracted stall speed estimate of 59 kts.

3.2 Structural Flight Envelope

In the certification criteria outlined in FAR Part 23 [9], airplanes are categorized according to the type of maneuvers and load factors, n, allowed. The categories and associated design load factors are shown in Table 5.

The Mustang II wing was designed for acrobatic maneuvers and load

factors at a weight of 1350 lbs which results in an average unit wing loading (W/S) of 83.51 lb/ft^2 for the 97.1 ft^2 wing. The relationship between the weight and equivalent load factor for the proposed 141 ft^2 wing when limited to the an 83.51 lb/ft^2 average unit load distribution is shown in Figure 9. The proposed 141 ft^2 wing would be capable of almost 5 g's at the proposed 2400 lbs design weight, or an acrobatic category load factor of 6 g's at 1950 lbs while remaining within existing Mustang II wing component limitations.

The aircraft structural flight envelope depicts the functional relationship between the aircraft flight speed and allowable load factor, n. The sample V-n diagram shown in Figure 10 identifies some of the most important design points. Points A, D, E, and G represent the minimum conditions under FAR Part 23 for which a certified, single-engine aircraft weighing 6000 lb, or less, must be

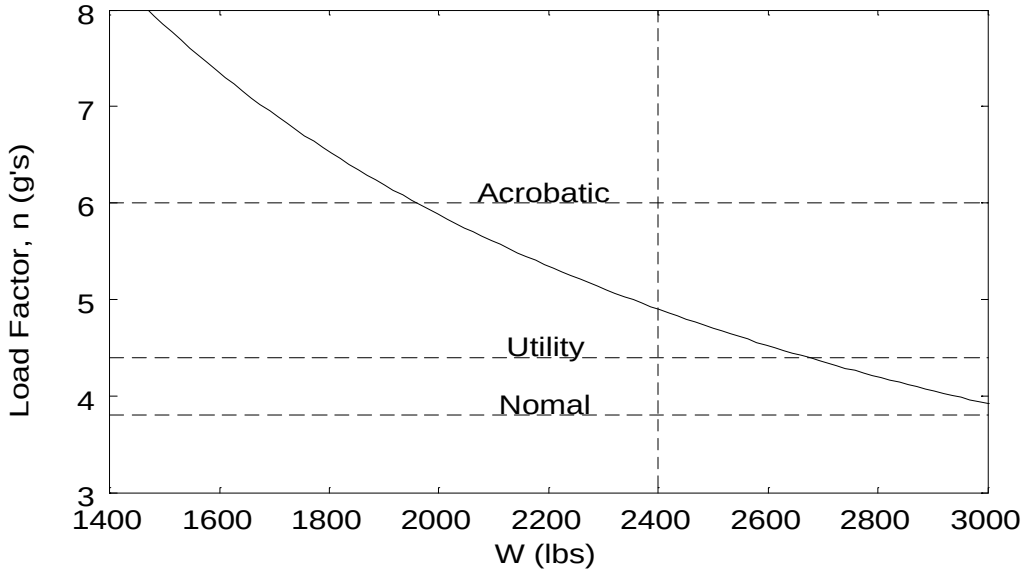

Figure 9. Load Factor Variation with Weight (W/S = 83.51 lb/ft^2).

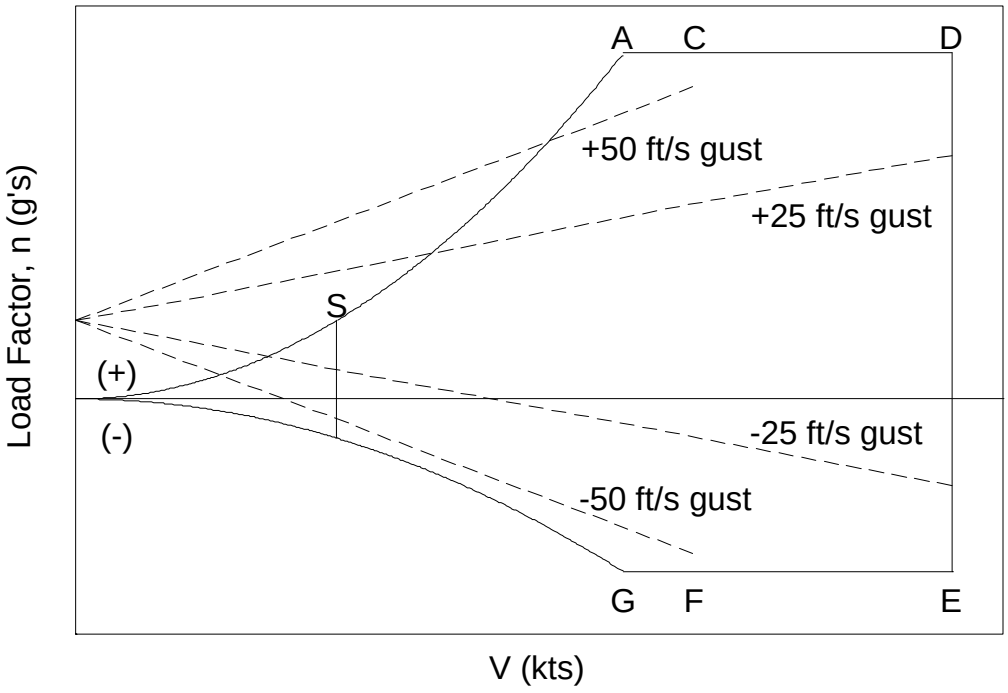

Figure 10. Sample V-n Diagram.

designed and tested. The line segment A-D represents the maximum allowable positive maneuvering load factor, n_1, and the line segment G-E represents the maximum allowable negative maneuvering load factor, n_3. The vertical line segment at point S represents the stall speed, V_S, with flaps retracted at the design weight. The curved line segment, S-A, represents the possible, lift-limited, load factors at speeds below the maneuvering speed, V_A. The design cruise speed, V_C, is coincident with both points C and F and represents the maximum speed at which an encounter with a positive or negative 50 ft/s gust will not result in a load factor exceeding n_1 or n_3 respectively. The line segment

D-E represents the design dive speed, V_D, which is the maximum speed at which the airplane is designed to fly. Minimum permissible values of the design dive speed are specified by FAR Part 23. Additionally, the design dive speed must be limited such that an encounter with either a positive or negative 25 ft/s gust will not exceed the design load factors n_1 and n_3.

FAR Part 23 specifies acceptable methods for establishing the minimum design speeds, and the speeds for the proposed airplane are:

$$V_A = 15\sqrt{n_1 \frac{W}{S}} = 130\,\text{kts}$$

$$V_C = 17\sqrt{n_1 \frac{W}{S}} = 147\,\text{kts}$$

$$V_D = 24\sqrt{n_1 \frac{W}{S}} = 208\,\text{kts}$$

The gust loads must additionally be checked to determine what limitations they might impose on the basic flight envelope at the V_C and V_D speeds. The load factor caused by a gust, U_{de}, is defined [9] as:

$$n = 1 + \frac{K_g U_{de} V a S}{498 W}$$

where:

$$K_g = \frac{0.88 * \mu_g}{5.3 + \mu_g} \quad \text{and} \quad \mu_g = \frac{2 * W}{\rho * g * \bar{c} * S * a} \quad \text{and} \quad a = \frac{2 * \pi * A}{A + 2}$$

The resulting gust load factors, shown in Table 6, are less than the basic design utility load factor of 4.4 and, therefore, need no further consideration.

Implicit to the calculation of V_A is an assumption about the maximum

Table 6. Gust Load Factors [9].

V	U_{de} (ft/sec)	n (g's)
V_C	50	3.98
	-50	-1.98
V_D	25	3.1
	-25	-1.1

achievable wing normal force coefficient, because the line S-A in Figure 10 is a lift limited (i.e. stall) condition. This means that a relationship between V_S and V_A is:

$$V_S = \frac{V_A}{\sqrt{n_1}} = 62\,\text{kts}$$

The 62 kts stall speed estimate above agrees reasonable well with the 59 kts estimate made previously based on performance estimates. This favorable comparison indicates that the estimated total lift coefficient for the proposed airplane is consistent with the default values used in FAR Part 23. Although the 59 kts estimate for V_S is more optimistic from a performance perspective, the resulting Utility category V_A, of 124 kts is more conservative from a structural perspective than the 130 kts minimum specified in FAR Part 23. In summary, the resulting structural flight envelope is shown in Figure 11.

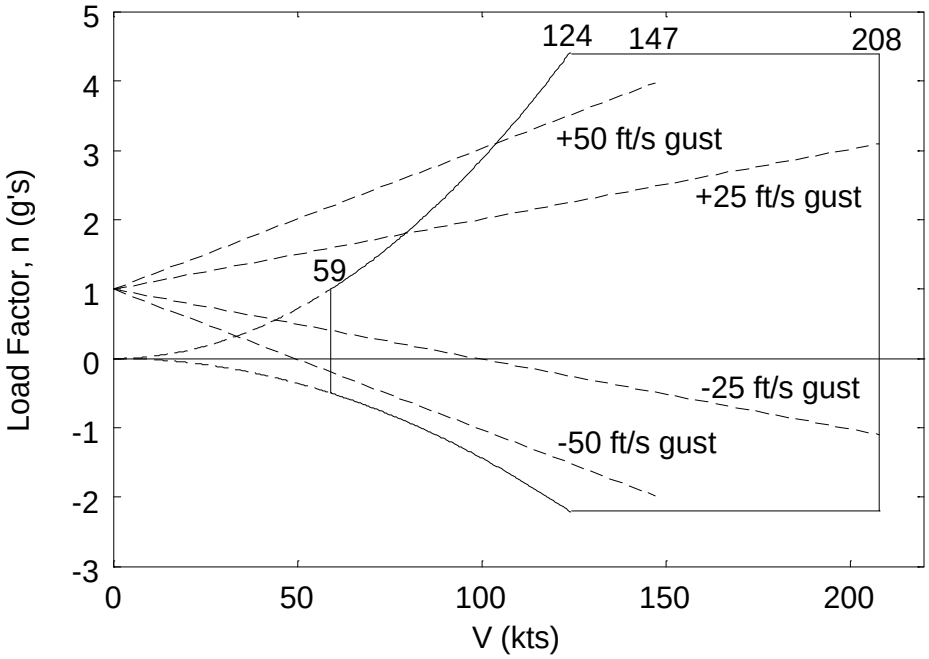

Figure 11. Proposed Structural Flight Envelope.

4. WING LOADS

4.1 Average Loads

Estimates for the wing lift and drag forces are necessary for airplane performance calculations, but estimates for body-axis normal and axial forces are necessary for airplane structural design. The relationship between axial, normal, lift and drag force coefficients is:

$$C_N = C_L \cos(\alpha) + C_D \sin(\alpha) \qquad 4.1$$

$$C_A = C_D \cos(\alpha) - C_L \sin(\alpha)$$

The lift characteristics of the proposed, relatively high aspect ratio wing will be generally linear over most of the angle of attack range [10]. Over the linear angle of attack range the average wing lift coefficient can be expressed [3] as:

$$C_{L_{wing}} = C_{L_\alpha} \cdot (\alpha - \alpha_{C_{L0}}) \qquad 4.2$$

where the wing lift curve slope [3] is:

$$C_{L_\alpha} = 2\pi \cdot \left(\frac{A}{A+2}\right) \qquad 4.3$$

Combining Equations 4.3 and 4.4 results in the equation for wing lift coefficient:

$$C_{L_{wing}} = 2\pi \cdot \left(\frac{A}{A+2}\right) \cdot (\alpha - \alpha_{C_{L0}}) \qquad 4.4$$

An estimate for the average wing drag coefficient may be obtained [3] using:

$$C_{D_{wing}} = C_{d_o} + \frac{C_{L_{wing}}^{\ 2}}{\pi \cdot A \cdot e} \qquad 4.5$$

Then for any angle of attack, the wing lift, drag, normal and axial force coefficients can be determined as shown in Figure 12.

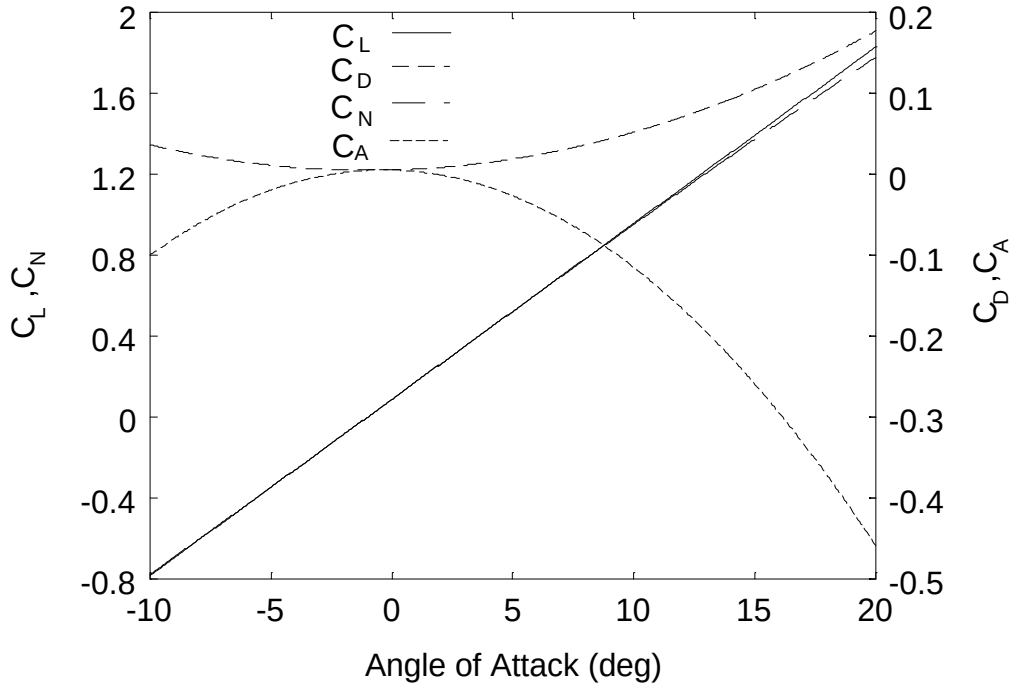

Figure 12. Force Coefficient Variation with Angle of Attack.

To correlate the force coefficients in Figure 12 to the points on the V-n diagram in Figure 11, some estimate for the associated angle of attack is needed. For any point on the V-n diagram:

$$\frac{2Wn}{\rho S V^2} = C_N \approx C_L \cdot \cos(\alpha) \approx C_L = C_{L_{wing}} + C_m \frac{\bar{c}}{l_t} \qquad 4.6$$

Combining 4.6 with 4.4 yields:

$$\frac{2Wn}{\rho S V^2} = 2\pi \cdot \left(\frac{A}{A+2}\right) \cdot (\alpha - \alpha_{C_{L0}}) + C_m \frac{\bar{c}}{l_t}$$

which can be solved for angle of attack:

$$\alpha = \left(\frac{2Wn}{\rho S V^2} - C_m \frac{\bar{c}}{l_t}\right) \cdot \left(\frac{A+2}{2\pi A}\right) + \alpha_{C_{L0}}$$

Table 7. Average Wing Aerodynamic Coefficients.

Condition	A	D	E	G
V (kts)	130	208	208	130
n (g's)	4.4	4.4	-2.2	-2.2
$C_{m_{wing}}$	-0.040	-0.038	-0.025	-0.020
α (deg)	15.3	6.1	-3.2	-7.9
$C_{L_{wing}}$	1.416	0.614	-0.188	-0.599
$C_{D_{wing}}$	0.108	0.024	0.007	0.024
$C_{N_{wing}}$	1.395	0.613	-0.188	-0.6
$C_{A_{wing}}$	-0.268	-0.04	-0.004	-0.060

Table 7 shows a summary of the average aerodynamic wing force coefficients for the proposed flight envelope.

4.2 Span-wise Load Distibution

Because of the aerodynamic losses at the tip of a wing with finite span, the span-wise distribution of the normalized local lift and drag coefficients will have characteristics similar to that shown in Figure 13. The basic airfoil moment coefficient will be assumed constant over the span. Distributing the span-wise normalized lift and drag coefficients over the proposed wing results in the span-wise unit coefficient distribution shown in Figure 14.

4.3 Outer Panel Loads

The outer wing panels of the proposed wing are structurally cantilevered, and the bending stress at the attachment due to shear loads is expected to

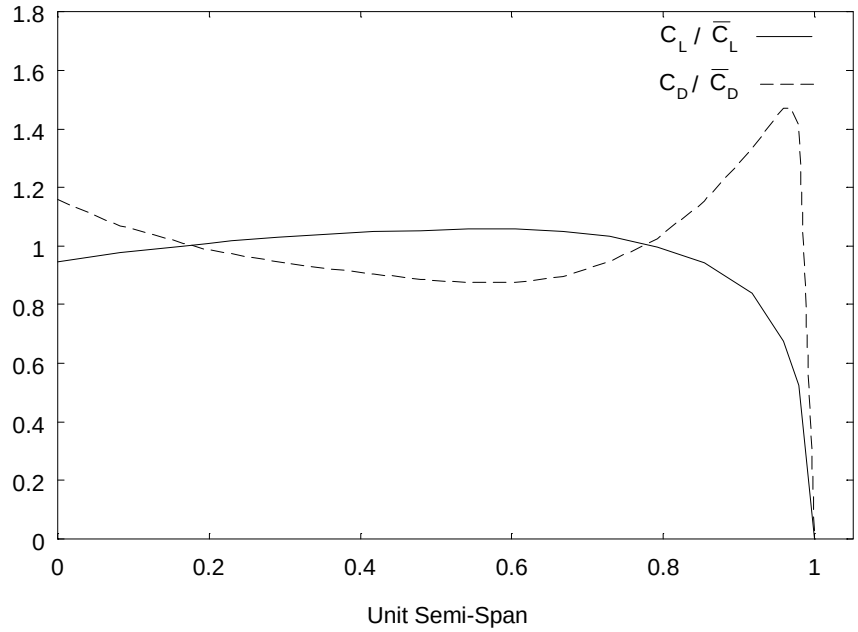

Figure 13. Span-wise Distribution of Normalized Lift and Drag Coefficients [3,10,12].

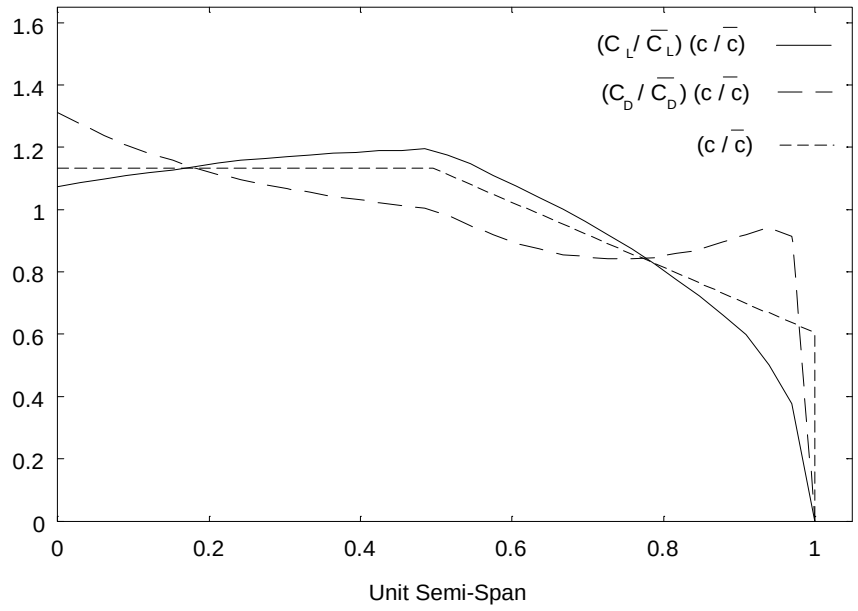

Figure 14. Span-wise Unit Coefficient Distribution.

dictate the wing structural limitations. Either condition A or D of the proposed flight envelope may be used to estimate the maximum wing shear load and associated wing bending moment. The shear load applied to the wing structure includes both the aerodynamic load associated with the normal-force coefficient (Table 7) and the inertia relief from the weight of the structure itself.

$$F_{shear} = F_N - F_{inertia\ relief}$$

For the calculated loads presented herein, the inertia relief was conservatively estimated considering only the aluminum wing skin structure. The resulting span-wise normal force and bending moment distributions are shown in Figures 15 and 16, respectively. Corresponding estimates for the Mustang II wing based on a 6 g, aerobatic-category load factor at 1350 lbs are shown, by comparison, to be nominally 10% higher. The Mustang II outer wing panels employ main spar flanges built up by laminating 0.125” thick aluminum strips that are 1.5” wide at the root and taper in width toward the tip. The discontinuities in the cross-sectional area at the end of each strip are responsible for the the saw-tooth bending stress distribution shown in Figure 17

One necessary change to the original Mustang II outer wing panel will be a larger aileron. With respect to FAR Part 23 wing load considerations, normal wing loads associated with aileron deflections, although unbalanced, are not considered to exceed 100% of the nominal maximum loading regardless of aileron span. The primary structural consequence of a larger aileron is more wing torsion. The section moment coefficient for that portion of the wing that includes the aileron may be calculated as:

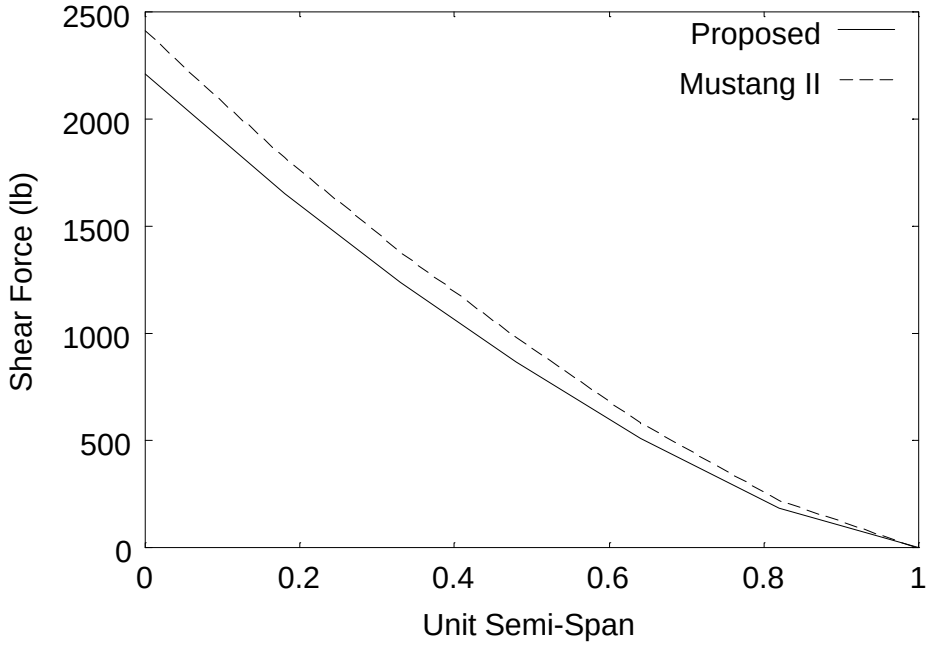

Figure 15. Wing Outer Panel Shear Force Distribution.

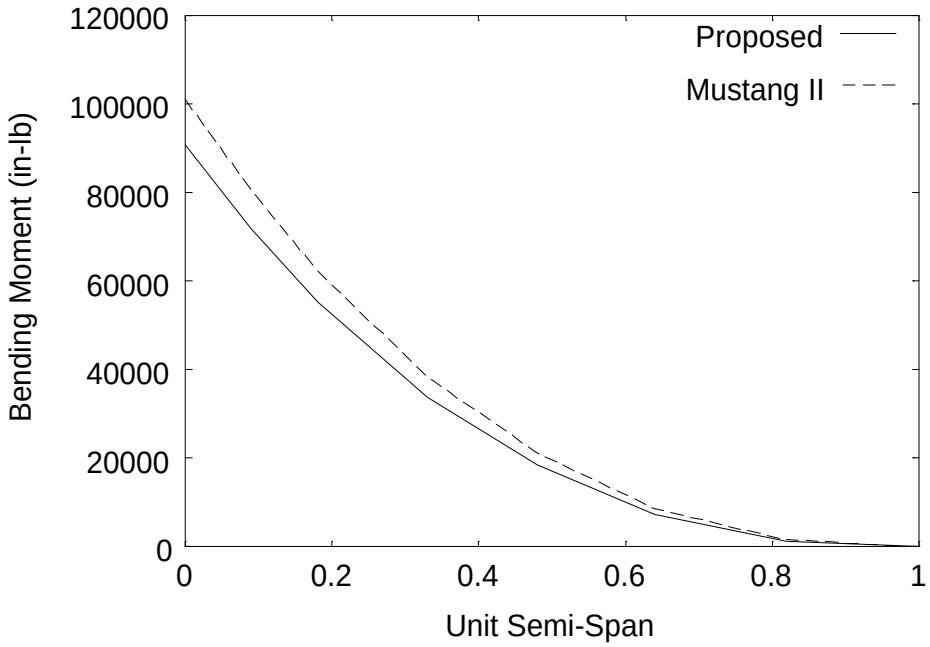

Figure 16. Wing Outer Panel Bending Moment Distribution.

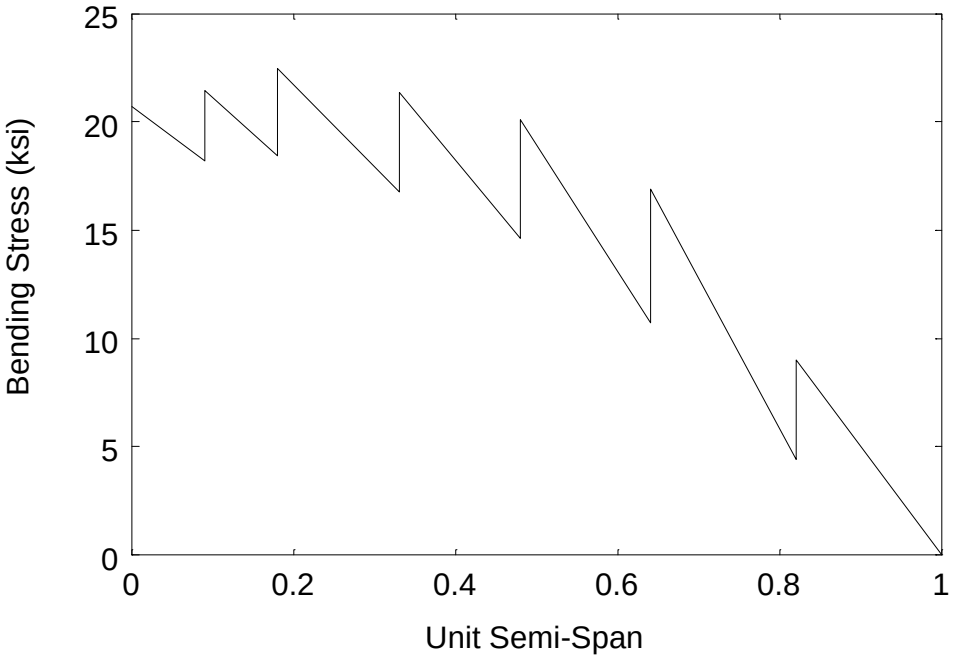

Figure 17. Wing Outer Panel Bending Stress Distribution.

$$C_m = C_{m_{nominal}} - \frac{0.01}{deg} \cdot \delta_{down}$$

Maximum aileron deflections are permitted for speeds up to Condition A of the flight envelope. The allowable aileron deflection decreases as the speed increases to Condition D. The critical speed/aileron-deflection combination was determined from FAR Part 23 as follows:

$$\Delta_p = \delta_{up} + \delta_{down}$$

$$\delta_{up} = 25\,deg \quad \text{and} \quad \delta_{down} = 15\,deg$$

For the condition at V_C:

$$\Delta_a = \frac{V_A}{V_C}\Delta_p = 35.3\,deg$$

$$\delta_a = \frac{\Delta_a}{\Delta_p}\delta_{down} = 13.2\,deg$$

For the condition at V_D:

$$\Delta_b = \frac{V_A}{V_D}\Delta_p = 12.5\,deg$$

$$\delta_b = \frac{\Delta_b}{\Delta_p}\delta_{down} = 4.7\,deg$$

Define:

$$K = \frac{(C_{m_{c/4}} - 0.01\cdot\delta_b)V_D^{\,2}}{(C_{m_{c/4}} - 0.01\cdot\delta_a)V_c^{\,2}} = 1.9 \qquad 4.7$$

Since K in Equation 4.7 is greater than 1.0, the δ_b condition at V_D is considered the critical case [1], and the incremental moment coefficient is:

$$\Delta C_{m_{c/4}} = -0.01\cdot\delta_b = -0.047$$

The aileron-deflected, outer panel wing torque was then estimated according to:

$$T = q\left(C_{m_{c/4}}\int_{y_o}^{\frac{b}{2}} c^2\,dy + \Delta C_{m_{c/4}}\int_{y_{aileron}}^{\frac{b}{2}} c^2\,dy\right)$$

Table 8 shows a comparison of the estimated maximum, aileron-deflected wing torsion for both the proposed wing and the Mustang II. The increased aileron span of the proposed wing combined with a 4% higher design speed results in a 40% increase in the outer panel wing torque which must be reacted by the panel attachments.

In order to estimate the reaction loads at the outer wing panel attachment,

Table 8. Outer Wing Panel Aileron-Deflected Torsion Estimate.

Airplane	V (kts)	Torque (ft-lb)
Proposed	208	-1210
Mustang II	200	-860

it was convenient to represent the distributed normal and axial loads as point loads. The chord-wise center of pressure, cp, is considered to act at 25% of the outer panel mac. An equivalent span-wise center of pressure, relative to the outboard panel attachment point, was determined according to:

$$y_{cp} = \frac{\int k \cdot c \cdot y \, dy}{\int k \cdot c \, dy}$$

where k is the span-wise distribution shown previously in Figure 13:

$$k_{lift}(y) = C_L / \bar{C}_L \text{ and } k_{drag}(y) = C_D / \bar{C}_D$$

so:

$$y_{cp_{lift}} = 0.413 \cdot b_o$$

$$y_{cp_{drag}} = 0.487 \cdot b_o$$

The outer wing panel, vertical z-axis, attachment reaction loads on the forward (main) and aft spars were determined by summing the normal forces and associated moments about a lateral axis coincident with the forward spar centerline. The resulting system of equations may be written as:

$$\begin{bmatrix} -\frac{1}{F_N} & -\frac{1}{F_N} \\ \frac{0.05\bar{c}_o}{T} & \frac{\Delta X_{spars}+0.05\bar{c}_o}{T} \end{bmatrix} \begin{bmatrix} R_{fwd_z} \\ R_{aft_z} \end{bmatrix} = \begin{bmatrix} 1 \\ 1 \end{bmatrix}$$

Likewise, the outer wing panel, lateral y-axis, attachment reaction loads on the forward and rear spars were determined by summing the lateral forces and the axial-force-induced moments about a vertical axis coincident with the forward spar. The resulting system of equations may be written as:

$$\begin{bmatrix} 1 & 1 \\ 0 & \frac{\Delta x_{spar}}{D\cdot\cos(\alpha)\cdot y_{ac_{drag}} - L\cdot\sin(\alpha)\cdot y_{ac_{lift}}} \end{bmatrix} \begin{bmatrix} R_{fwd_y} \\ R_{aft_y} \end{bmatrix} = \begin{bmatrix} 0 \\ 1 \end{bmatrix}$$

The longitudinal, x-axial wing/fuselage and wing/strut reactions were determined from:

$$R_{fwd_x} + R_{aft_x} - F_A = 0$$

The relative distribution between the forward and aft axial reactions depends on the relative stiffness of the wing attachment fittings. Since the main spar fitting of the Mustang II outer wing panel is significantly more substantial than the aft fitting, the aft attachment was assumed to carry none of the axial reaction. The axial reaction was then estimated as:

$$R_{fwd_x} = -F_A$$

Table 9 shows the resulting outer panel wing attachment reaction load components. In addition to the primary flight envelope design points, two additional aileron-deflected conditions, δ_b at condition D and δ_{15} at condition A, were also examined. For these aileron-deflected calculations, the incremental

Table 9. Outer Wing Panel Reaction Load Components.

	A	D	E	G	D(δ_b)	A(δ_{15})
R_{fwd_x} (lb)	415	130	31	113	130	415
R_{fwd_y} (lb)	646	193	42	176	193	646
R_{fwd_z} (lb)	-2288	-2100	1326	1223	-1839	-1965
R_{aft_x} (lb)	0	0	0	0	0	0
R_{aft_y} (lb)	-646	-193	-42	-176	-193	-646
R_{aft_z} (lb)	72	-109	-294	-159	-369	-251

drag force associated with the relatively small (5-15 deg.) aileron deflections was ignored and resulted in a conservative axial force estimate.

Combined attachment loads, the basis for sizing attachment hardware, have been calculated as:

$$P_i = \sqrt{(R_{i_y})^2 + (R_{i_z})^2}$$

The resulting combined attachment loads are summarized in Table 10. Note that the largest combined reaction on the forward attachment occurs at condition A while the worst case for the aft attachment is condition A(δ_{15}).

4.4 Total Wing Attachment Reaction Loads

By considering only the that portion of the wing outboard of the fuselage, the lift and drag force lateral centers of pressure, referenced to the fuselage center line, were determined to be:

Table 10. Outer Wing Panel Combined Reaction Loads

	A	D	E	G	D(δ_b)	A(δ_{15})
R_{fwd} (lb)	2377	2108	1327	1236	1849	2068
R_{aft} (lb)	650	221	297	237	416	693

$$y_{cp_{Lift}} = 0.497 \cdot \frac{b}{2}$$

$$y_{cp_{Drag}} = 0.523 \cdot \frac{b}{2}$$

The wing strut attachment is coincident with the main wing spar and located at:

$$y_{strut} = 0.444 \cdot \frac{b}{2}$$

The vertical, z-axis, wing/fuselage and wing/strut attachment reaction loads on were determined by summing the normal forces and associated moments about a lateral axis coincident with the forward spar centerline. The resulting system of equations may be written as:

$$\begin{bmatrix} -\frac{1}{F_N} & -\frac{1}{F_N} & -\frac{1}{F_N} \\ 0 & 0 & -\frac{(y_{strut}-(0.5\cdot w_{fuselage}))}{(y_{cp_{Lift}}-(0.5\cdot w_{fuselage}))} \\ \frac{0.05\bar{c}}{T} & \frac{\Delta X_{spars}+0.05\bar{c}}{T} & 0 \end{bmatrix} \begin{bmatrix} R_{fwd_z} \\ R_{aft_z} \\ R_{strut_z} \end{bmatrix} = \begin{bmatrix} 1 \\ 1 \\ 1 \end{bmatrix}$$

The lateral, y-axis, wing/fuselage and wing/strut reactions were determined by summing the lateral forces and the axial-force-induced moments about a

vertical axis coincident with the forward spar. The strut geometry dictates that:

$$R_{strut_y} = -R_{strut_z} \cdot \frac{\Delta y_{strut}}{\Delta z_{strut}}$$

and the remaining reactions may determined from the system of equations:

$$\begin{bmatrix} \frac{\Delta z_{strut}}{\Delta y_{strut} \cdot R_{strut_z}} & \frac{\Delta z_{strut}}{\Delta y_{strut} \cdot R_{strut_z}} \\ 0 & \frac{\Delta x_{spar}}{L \cdot \sin(\alpha) \cdot y_{ac_{lift}} - D \cdot \cos(\alpha) \cdot y_{ac_{drag}}} \end{bmatrix} \begin{bmatrix} R_{fwd_y} \\ R_{aft_y} \end{bmatrix} = \begin{bmatrix} 1 \\ 1 \end{bmatrix}$$

The longitudinal, x-axis, wing/fuselage and wing/strut reactions were determined from a combination of strut geometry:

$$R_{strut_x} = R_{strut_z} \cdot \frac{\Delta x_{strut}}{\Delta z_{strut}}$$

and summing axial forces:

$$R_{fwd_x} + R_{aft_x} + R_{strut_x} + F_A = 0$$

The relative distribution between the forward and aft reactions depends on the as-yet-undetermined relative stiffness of the wing attachment fittings. Initially, the aft attachment will be assumed to carry none of the axial reaction

Table 11 shows the resulting wing attachment reaction load components. In addition to the primary flight envelope design points, the critical aileron-deflected condition was also examined. For these calculations, the incremental drag force associated with the small (less than 5 deg) critical aileron deflection is considered insignificant

As with the outer wing panel, the combined forward and aft wing/fuselage

Table 11. Wing Reaction Load Components.

	A	D	E	G	D(δ_b)	A(δ_{15})
R_{fwd_x} (lb)	1178	574	-66	100	574	1178
R_{fwd_y} (lb)	-10440	-8156	3088	2582	-8156	-10440
R_{fwd_z} (lb)	1081	1491	90	-238	1751	1404
R_{aft_x} (lb)	0	0	0	0	0	0
R_{aft_y} (lb)	3293	1024	245	854	1024	3293
R_{aft_z} (lb)	-361	-772	-426	-109	-1032	-683
R_{strut_x} (lb)	-294	-293	-137	-141	-293	-294
R_{strut_y} (lb)	7149	7132	-3333	-3437	7132	7149
R_{strut_z} (lb)	-5315	-5302	2478	2555	-5302	-5315

attachment loads have been calculated as:

$$P_i = \sqrt{(R_{i_y})^2 + (R_{i_z})^2}$$

and the total strut load has been calculated as:

$$P_{strut} = \sqrt{(R_{strut_x})^2 + (R_{strut_y})^2 + (R_{strut_z})^2}$$

The resulting combined attachment loads are summarized in Table 12. Note that the largest combined reaction on both the forward and rear attachments occurs at condition A(δ_{15}).

Table 12. Wing Combined Reaction Loads.

	A	D	E	G	D(δ_b)	A(δ_{15})
R_{fwd} (lb)	10496	8291	3089	2593	8342	10534
R_{aft} (lb)	3313	1282	491	861	1454	3363
R_{strut} (lb)	8913	8892	4155	4284	8892	8908

5. WING STRUCTURE

5.1 General

The mechanical properties of the materials planned for use in the proposed construction are shown in Table 13. Except where indicated, a design safety factor of 1.5 has been applied to ultimate stress values to determine allowable design stress levels. Note that the references to normal stresses that follow are not related to the aerodynamic normal-force coefficients discussed in the previous chapter.

5.2 Outboard Wing Panel Attachments

Since the outer wing panel normal force and bending moments for the proposed airplane were shown in Figures 15 and 16 to be smaller than for the Mustang II, the existing Mustang II main spar attachment should be adequate for the proposed airplane without modification.

The rear spar attachment of the Mustang II outer wing panel uses the

Table 13. Material Mechanical Properties
(values given in ksi) [12,13]

	σ_{tu}	σ_{ty}	σ_d	τ_u	τ_d	σ_{bu}
2024-T3 alclad sheet	56	37	37	34	22.6	82
2024-T3 aluminum plate	62	40	40	38	25.3	90
4130 normalized steel	90	70	60	55	36.6	140
AN Bolt	125			75	50	
AD Rivet	38			26	17.3	

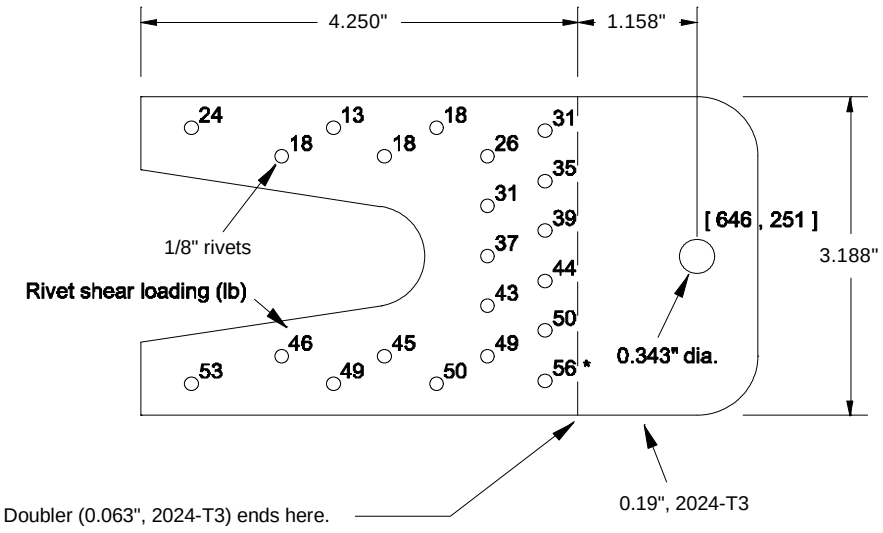

Figure 18. Mustang II Aft Spar Attachment Fitting [4].

fitting shown in Figure 18. The fitting and a 20” long, 0.063” thick doubler are attached to the 0.040” thick rear spar channel using 1/8” rivets. The fitting was evaluated using the loading conditions shown in Table 9. A macro program interfacing with the commercial DesignCad 3D Max drafting software was written to determine the fastener shear load associated with any arbitrary fastener arrangement and applied loading. The fastener shear load is the geometric sum of the direct loading superimposed with the moment-induced load (associated with the load eccentricity) proportional to the fastener distance to the instantaneous center of rotation [14]. With respect to rivet shear loading, the condition A(ō15) was determined to be the critical case, and the resulting rivet shear loads are shown superimposed in Figure 18. Using the data in Table 13, the design shear strength of the 1/8” rivets is 212 lbs, nearly 4 times the

maximum value shown in Figure 18. The rear spar channel is made from 0.040" 2024-T3 aluminum, and when combined with the 0.063" doubler plate the maximum bearing stress on the rivet holes would be:

$$\sigma_{b_{rivet}} = \frac{F_{rivet_{max}}}{d_{rivet} \cdot t_{plate_{min}}} = 4350 \text{ psi}$$

or about 19% of the design value.

The maximum normal stress on the fitting was calculated as the sum of bending stress associated with the vertical reaction component and the axial stress associated with the lateral reaction component. Considering all of the cases in Table 9, the maximum normal stress occurred at condition A(δ15) and was estimated as:

$$\sigma_{total} = \sigma_{bending} + \sigma_{axial} = 26.75 \text{ ksi}$$

which is about 67% of the design value.

5.3 Inboard Wing Panel Main Spar

The main inboard-panel wing spar will be constructed using the same basic technique as the outboard wing panel. The main spar top and bottom flanges will be riveted to a common 0.040" thick c-channel shear web with a nominal rivet spacing of 1 inch. The shear web will include a 0.063" doubler. Like the Mustang II, the top and bottom spar flanges will be laminated from 1.5" wide by 0.125" thick strips of 2024-T3 aluminum. The Mustang II inboard/outboard panel attachment will be used unchanged. Details of the main inboard wing spar are shown in Figure 19.

The shear force and bending moments on the the inboard wing panel are

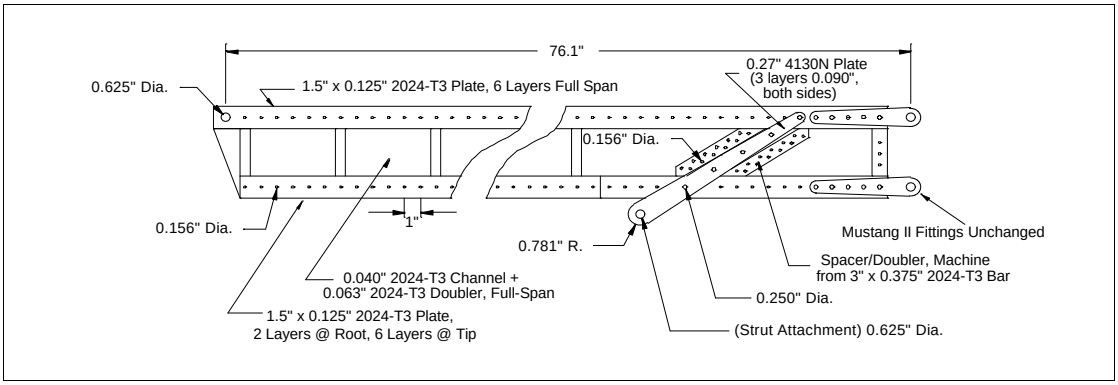

Figure 19. Inboard Wing Panel, Main Spar Details.

shown in Figure 20. Both the shear and moments peak at the strut attachment. Note that the moment at the fuselage attachment does not go to zero, because the main spar/fuselage attachment is not coincident with the spar neutral axis The number of cap strips on the top flange is constant at 6. The number of cap strips on the bottom flange at each span station was based on maintaining stress levels at or below the maximum level at the strut attachment. The resulting span-wise stress distribution is shown in Figure 21.

The shear flow along the spar cap rivet line is maximum where the shear force is maximum and coincides with the strut attachment point. An approximate but conservative estimate for the maximum shear flow is:

$$q_{max} = \frac{V_{max}}{h} = \frac{2780 \text{ lb}}{4.8 \text{ in}} = 580 \text{ lb/in}$$

Given a nominal rivet spacing of 1 inch, the maximum rivet loading would be:

$$F_{rivet} = q_{max} \cdot 1 \text{ inch} = 580 \text{ lb}$$

The minimum rivet diameter, based on the design bearing stress for the 0.103”

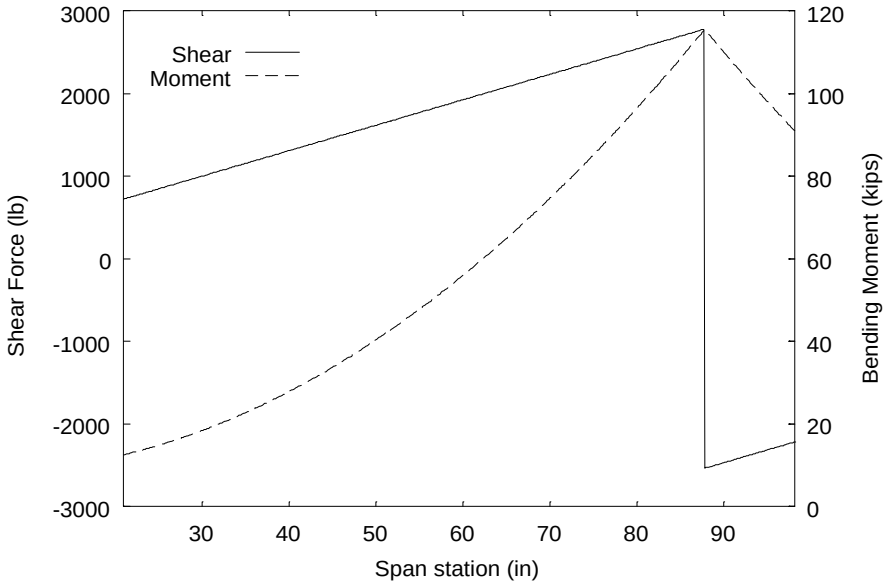

Figure 20. Inboard Wing Panel, Shear and Moment Diagram.

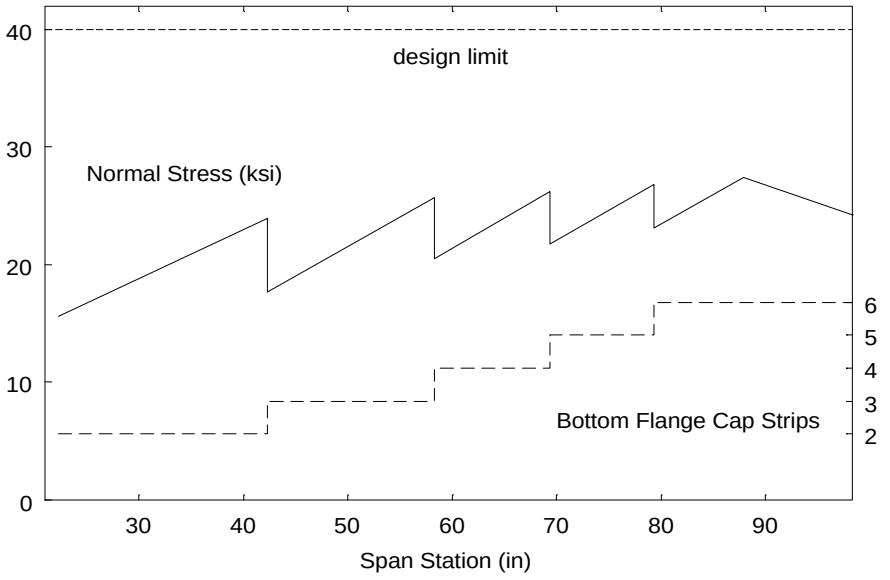

Figure 21. Inboard Wing Panel, Span-wise Normal Stress Distribution.

thick shear web, would be:

$$d_{min} = \frac{F_{rivet}}{\sigma_y \cdot t_{web}} = 0.157 \text{ inch} = 5/32 \text{ inch}$$

Since the spar caps are laminated on both sides of the shear web, a double shear condition exists on the rivet. Using the data in Table 13, the design shear strength of the 5/32" rivets in double shear is 660 lbs, which is 13% greater than the estimated maximum rivet loading.

The main spar shown in Figure 19 includes vertical shear web stiffeners spaced nominally 6" apart on one side only. The stiffeners are 5/8" wide and the thickness varies with the spar cap thickness from 1/8" at the root to 3/8" near the strut attachment. With respect to shear web buckling, the allowable shear stress is [12,13]:

$$\tau_{allowable} = K_s \cdot E \cdot \left[\frac{t_{web}}{h'}\right]^2 = 43{,}400 \ psi$$

where K_s was assumed to be 9.425 based on an average of values associated with either clamped or simply supported edges for the equivalent sheet between the stiffeners. The maximum estimated shear stress on the shear web is:

$$\tau_{max} = \frac{V_{max}}{h' \cdot t_{web}} = 5623 \ psi$$

which is considerably less than the allowable.

5.4 Wing/Strut Attachment

The wing/strut attachment is made of flat 4130N steel plates on both sides of the main spar resulting in a double shear condition on the attachment bolt. Design of the actual fitting and primary attachment hardware included an additional factor of safety:

$$k_{fitting} = 2$$

The minimum diameter for the AN attachment bolt is:

$$d_{min} = \sqrt{\frac{2 \cdot R_{strut} \cdot k_{fitting}}{\pi \cdot \tau_d}} = 0.476 \text{ inch}$$

Selecting a standard 5/8" bolt, the total minimum fitting thickness, based on allowable bear stress, can be determined from:

$$t_{min} = \frac{R_{strut} \cdot k_{fitting}}{d_{bolt} \cdot \sigma_d} = 0.475 \text{ inch}$$

By using 3 laminations of 0.090" plate on each side of the spar, each fitting is 0.27" thick for a total composite thickness of 0.54". If the fitting width is 2.5 times the bolt diameter, then the minimum equivalent cross section width coincident with the bolt center line is 1.5 times the bolt diameter. Since the fitting end has a radius finish, the tear-out cross section has the same dimensions,but in a different plane. Therefore:

$$\tau_{\text{tear-out}} = \sigma = \frac{R_{strut}}{t_{fitting} \cdot (2.5-1) \cdot d_{bolt}} = 17{,}610 \text{ psi}$$

In this case the tear-out shear stress is the more critical condition in proportion to the allowable but is still less than half of the design stress level in Table 13.

The wing strut attachment fittings shown in Figure 19 attach to the main spar with 1/4” AN bolts in the upper and lower spar cap and 3, 1/4” AN bolts in a spacer between the cap strips on each side of spar. The spar fitting spacer is machined from 2024-T3 aluminum plate to be consistent with the total thickness of the cap strips and results in uniform attachment bolt loading. The shear stress on the 1/4” bolts attaching the fitting to the spar is:

$$\tau_{bolt} = \frac{(1/2)\cdot R_{strut}}{5\cdot A_{bolt}} = 18{,}160 \text{ psi}$$

The bearing stress on the bolt holes is:

$$\sigma = \frac{R_{strut}}{5\cdot t_{cap}\cdot d_{bolt}} = 9{,}510 \text{ psi}$$

Three fifths of the strut load are applied to the 2 spar fitting spacers, which are riveted to the shear web with 24, 5/32” rivets. The bearing stress on the 0.103” shear web is:

$$\sigma = \frac{(3/5)\cdot R_{strut}}{t_{web}\cdot d_{rivet}\cdot 24} = 14{,}260 \text{ psi}$$

The thickness of the spacer at the rivet line is 1/8”, thicker than the shear web, and requires no additional check. The shear on the rivets is:

$$\tau_{rivet} = \frac{(1/2)\cdot(3/5)\cdot R_{strut}}{12\cdot A_{rivet}} = 5{,}810 \text{ psi}$$

5.5 Forward Wing/Fuselage Attachment

The fuselage fitting for the forward fuselage/wing attachment will provide a double shear condition. Based on the maximum combined loading shown in

Table 12 for the forward fuselage/wing attachment the minimum bolt size was determined to be:

$$d_{min} = \sqrt{\frac{2 \cdot R_{fwd} \cdot k_{fitting}}{\pi \cdot \tau_d}} = 0.518 \text{ inch}$$

If the bolt is sized up to 5/8", then the minimum wing fitting thickness can be determined based on bearing stress according to:

$$t_{min} = \frac{R_{fwd} \cdot k_{fitting}}{d_{bolt} \cdot \sigma_d} = 0.843 \text{ inch}$$

The 6 1/8" thick cap strips combined with the 0.040" channel and 0.063" doubler result in a combined thickness of 0.853" providing a small margin of safety.

5.6 Aft Wing/Fuselage Attachment

Like the outboard wing panel, the aft inboard wing spar is built from a 0.040" channel. The aft fuselage/wing attachment fitting will also utilize a double shear design and the minimum bolt diameter was determined to be:

$$d_{min} = \sqrt{\frac{2 \cdot R_{aft} \cdot k_{fitting}}{\pi \cdot \tau_d}} = 0.293 \text{ inch}$$

In practice, an equivalent bolt diameter of 11/16" will be used to take advantage of standard hardware available for the Cessna 100 series airplanes. Cessna uses an 11/16" steel bushing on each side of the fitting with an eccentric 7/16" hole for the bolt that joints the bushings. The eccentricity allows the bushing to be rotated into one of two positions providing some minor adjustment to the relative angle of attack of the wing panel to compensate for lateral rigging

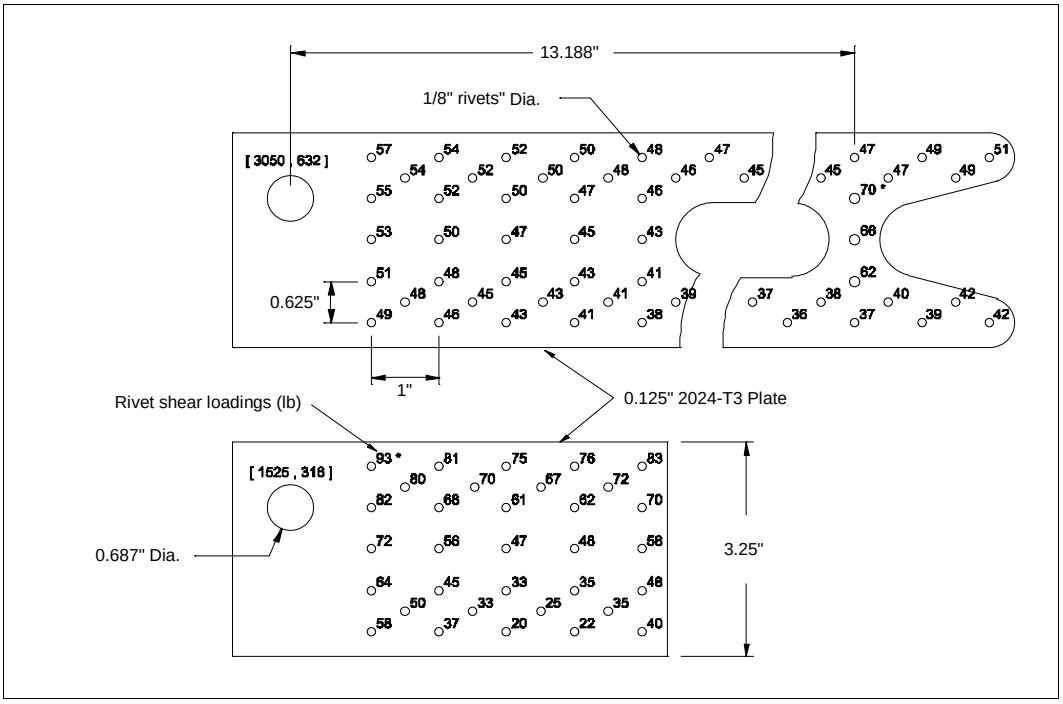

Figure 22. Inboard Wing Panel, Aft Spar Attachment Fitting Rivet Loads.

errors. Using the 11/16” bushing, the minimum thickness of the fitting was determined to be:

$$t_{min} = \frac{R_{aft} \cdot k_{fitting}}{d_{bushing} \cdot \sigma_d} = 0.244 \text{ inch}$$

By using the reinforcement structure shown in Figure 22 made from laminated 1/8”, 2024-T3 plate, the total fitting thickness is 0.290”. Considering the loading shown in Table 11 and adjusted by the relative thickness of the lamination, the resulting maximum rivet loading reacted by the 0.040” channel is shown to be 70 lb, and the associated bearing stress for a 1/8” rivet is:

$$\sigma_{bearing} = \frac{F_{rivet}}{t_{channel} \cdot d_{rivet}} = 14{,}000 \text{ psi}$$

and shear stress is:

$$\tau_{rivet} = \frac{F_{rivet}}{A_{rivet}} = 5{,}770 \text{ psi}$$

Likewise, the maximum rivet load on the smaller doubler plate is shown to be 93 lb, with bearing and shear stress of 5,950 psi and 7,580 psi, respectively.

6. FUSELAGE STRUCTURE

6.1 Steel Cabin Frame

The proposed steel frame cabin structure is shown in Figure 23. Analysis of the frame structure was accomplished using finite element methods. Although limited to beam and truss elements, the gbeam finite element analysis (FEA) software proved well suited to the frame analysis herein. The finite element model of the fuselage structure is shown in Figure 24 Note the simplification made to the aft fuselage to simulate the semi-monocoque aluminum tail cone. The CAD model of the cabin structure included the tube centerlines which were easily imported into the gbeam software. The baseline FEA model utilized a single tube size, 7/8” diameter with a 0.032” wall thickness.

The model structure was constrained axially and vertically at the strut/fuselage attachments (nodes 22 and 25) and constrained vertically and laterally at the end of the simulated tail cone (node 50). The simulated loading included the inertia of the steel structure plus passenger, engine/propellor and wing reaction loads. Although the design load factor is 4.4, the simulated mass/inertia loads were conservatively simulated at a load factor of 6.6 to partially compensate for excluding applied loads associated with control systems, seats, instruments, etc. Three passengers were simulated at 1320 lb each (200 lb at 6.6 g's) with two in the forward seats and one in the rear seat. The engine/propellor combination was assumed to weight 3036 lb (460 lb. at

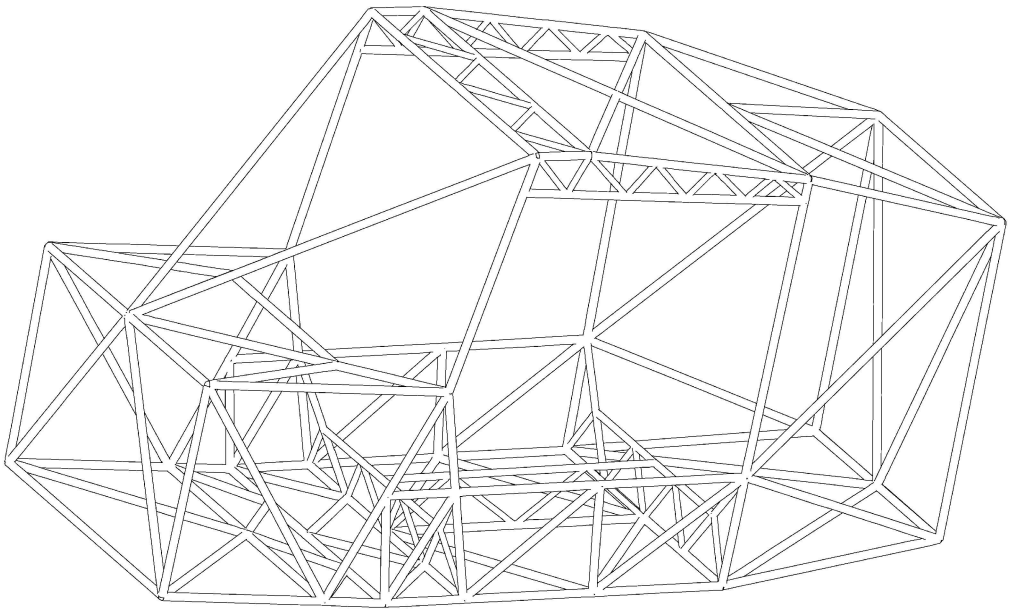

Figure 23. Cabin Steel Tubing Arrangement.

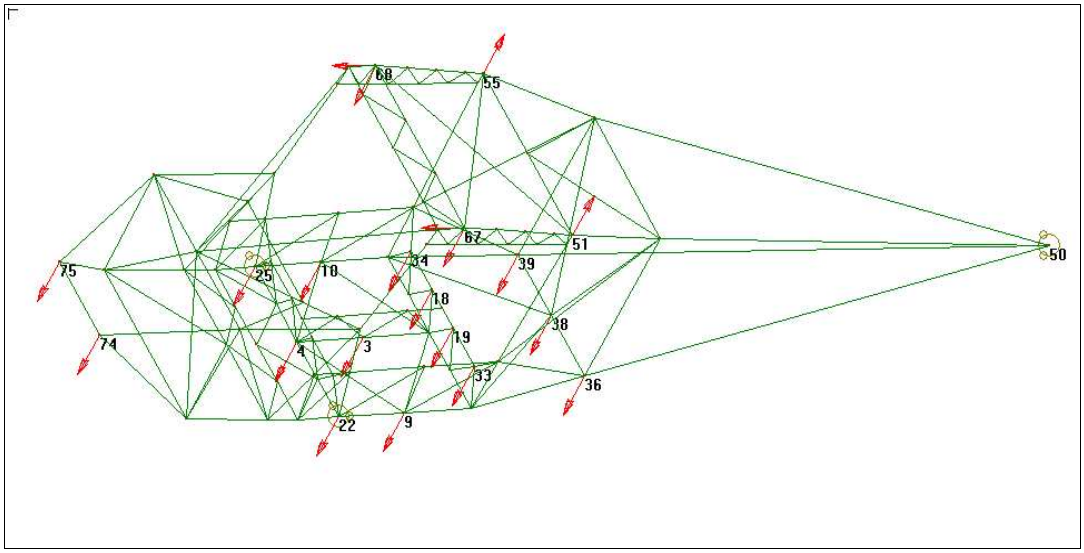

Figure 24. Finite Element Model.

6.6 g's). Worst case wing reaction loads from Table 11 were applied as a single, composite load case. The loads were discretely applied to a limited number of nodes on the FEA model shown in Figure 24. A summary of the applied loads is shown in Table 14. Note the lateral (inboard/outboard) wing and strut reaction loads have initially been omitted but will be discussed separately in a later section.

The resulting vertical constraint reaction at each fuselage/strut attachment was 5285 lb which compares well with the 5315 lb predicted, vertical fuselage/strut attachment load shown in Table 11. The resulting axial loads and bending moments in each tube member are shown in Figures 25 and 26 respectively. The highest axial loads are shown to be in the front door post, but the associated axial stress in the 7/8” x 0.035” tubes is only 35.8 ksi, and the axial loads are all well below conservative limits associated with column buckling.

Figure 26 shows that only a few members near the front of the door

Table 14. Finite Element Model Applied Loads.

Node(s)	Axial (lb)	Lateral (lb)	Vertical (lb)
18,19,33,34,36,39	0	0	-165
9,10,22,25,38	0	0	-330
3,4	0	0	-660
74,75	0	0	-1518
67,68	-1180	0	-1751
51,55	0	0	1032

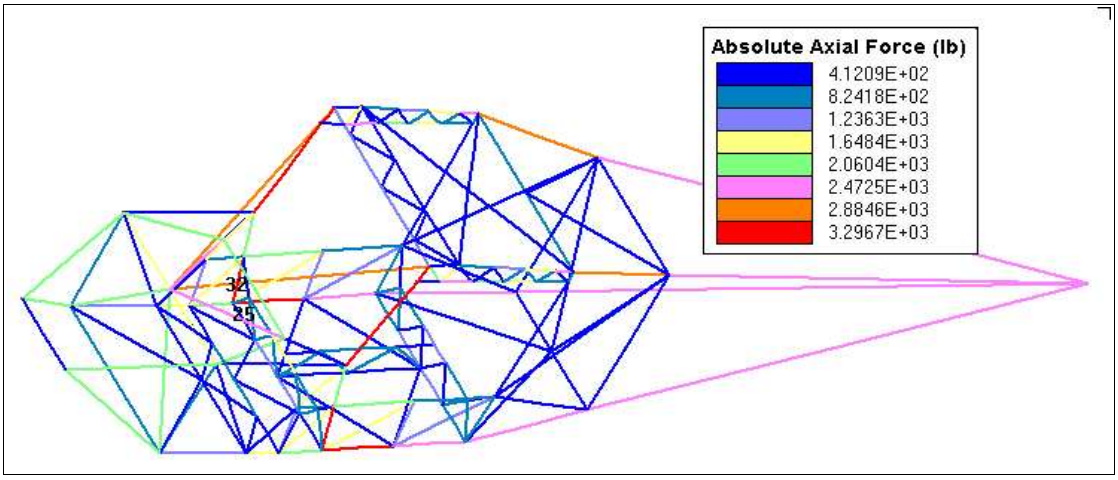

Figure 25. Tubing Axial Loads.

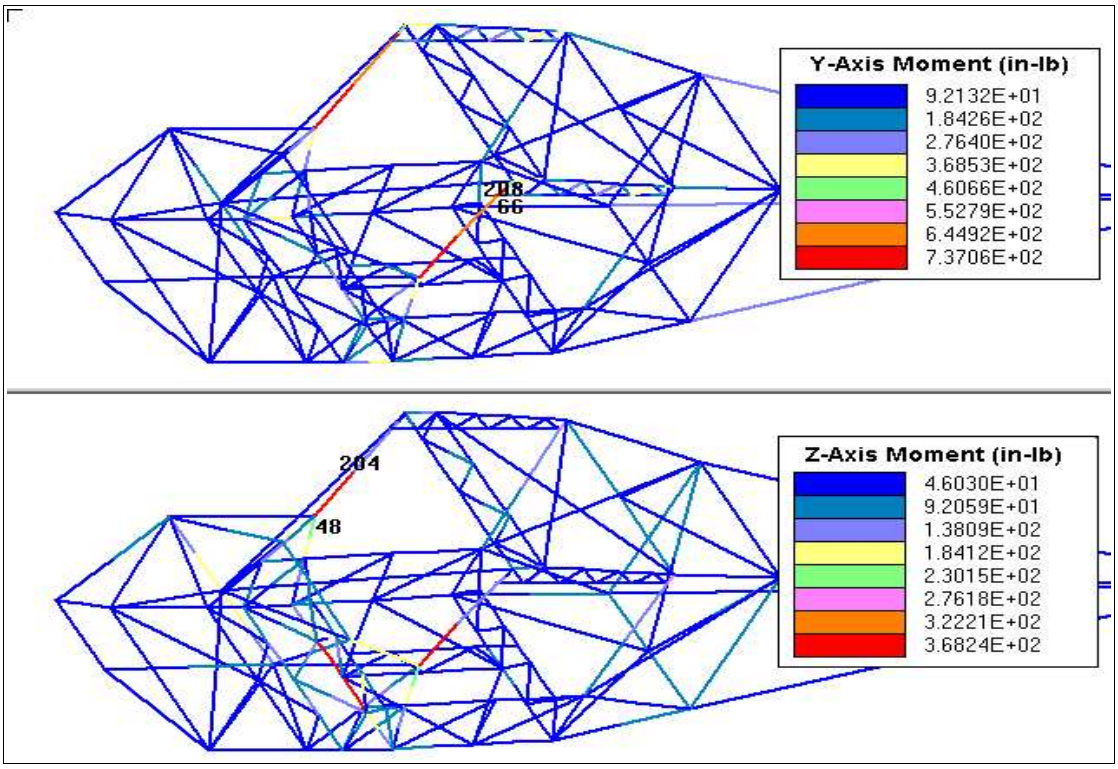

Figure 26. Tubing Moments.

opening experience much bending. This is likely related to the non-vertical front door post that was necessary to better enable entry and exist for the front-seat passengers. The gbeam software cannot not report combined stresses, so the output was post-processed to determine the combined normal stress according to:

$$\sigma_{combined} = \sigma_{axial} + \sqrt{\left(\sigma_{bending_{z\text{-}axis}}\right)^2 + \left(\sigma_{bending_{y\text{-}axis}}\right)^2}$$

The maximum combined normal stress was determined to be nominally 44 ksi with the distribution shown in Figure 27.

6.2 Special Consideration to Lateral Reactions

Because of their greater relative magnitude, the axial loads associated with the wing and strut lateral (inboard/outboard) reactions have been treated separately. Table 15 shows the critical design conditions, tubing size, and resulting stress levels associated with those members. The selected rectangular member cross-sections are somewhat uncommon in typical steel tube structures but proved well suited to the eventual attachment fitting design. The calculated stress levels are shown to be comfortably below the design values, but additional checks must be made for possible problems associated with column buckling in compression.

From Table 11, both the tube between the strut attachment (nodes 22 and 25) and the tube between the forward wing spar attachments (nodes 68 and 67) may experience significant compressive loads. From Figure 23, the tube (22-25) attached to the strut is shown stabilized in both the horizontal x-z and

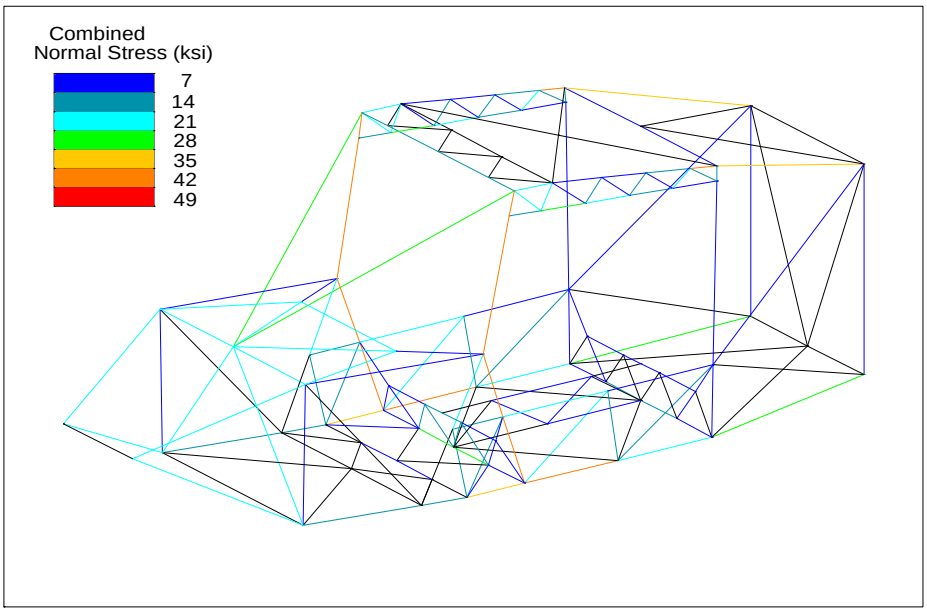

Figure 27. Combined Axial and Bending Normal Stress.

Table 15. Critical Fuselage Tube Properties.

Attachment	Axial Load (lb)	Cross Section	Axial Stress (ksi)
Wing (fwd)	-10,440	1.5”x1”x0.06”	-33.9
Wing (aft)	3,293	1.5”x0.75”x0.049”	15.6
Strut	7149	1.5”x1” x 0.065”	23.2

vertical y-z planes by other members and, therefore, needs no further consideration for buckling stability. Likewise, the tube attached to the main wing spar (67-68) is stabilized in the horizontal x-y plane by other members, so only the buckling stability in the vertical y-z plane needs to be considered.

The buckling stability of any tube is related to the critical buckling stress according to [13]:

$$F_{cr} = \frac{\pi^2 \cdot E}{(L/\rho)^2}$$

where:

$$\rho = \frac{I_x}{A}$$

is the radius of gyration and determines column stability for any given column length. By inspection, the radius of gyration of 1.5”x1”x0.065” rectangular tube in the plane of interest is nearly 10% greater than a 1.5”x0.065” round tube, so the rectangular cross-section should be able to resist slightly higher compression loads than the similar round tube. With conservative, unrestrained end conditions, the 1.5”x0.065” round tube can resist up to a 12,000 lb compression load. Using an end constraints more consistent with the welded construction, the maximum compression load is 17,000 lb., which provides a significant safety margin.

6.3 Fuselage Attachment Fittings

The proposed wing and strut attachment fittings are shown in Figures 28 and 29. A common design was possible for the both the main wing spar and the

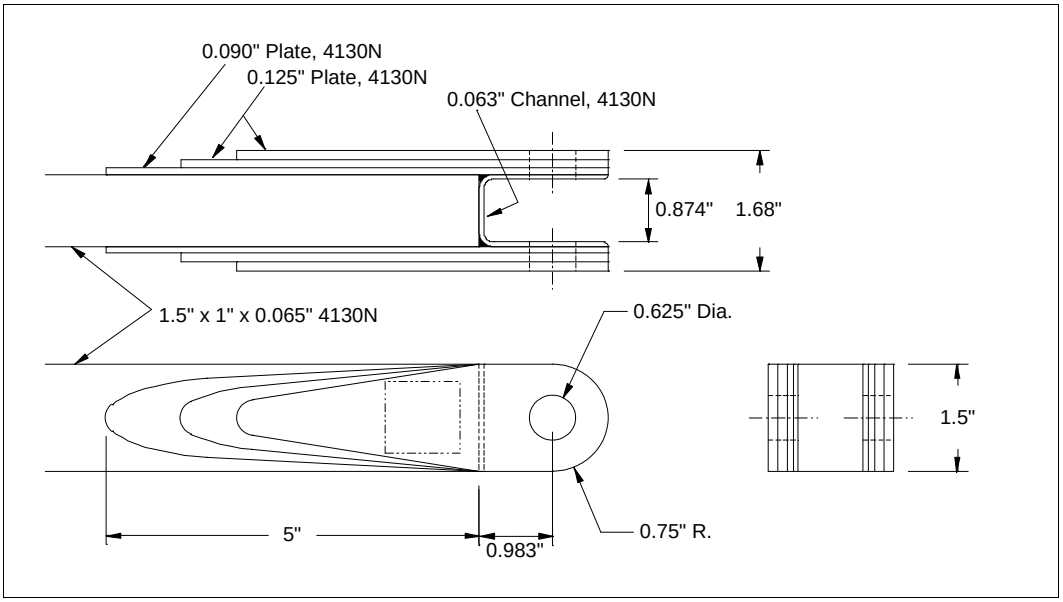

Figure 28. Fuselage Attachment Fitting, Strut and Main Wing Spar.

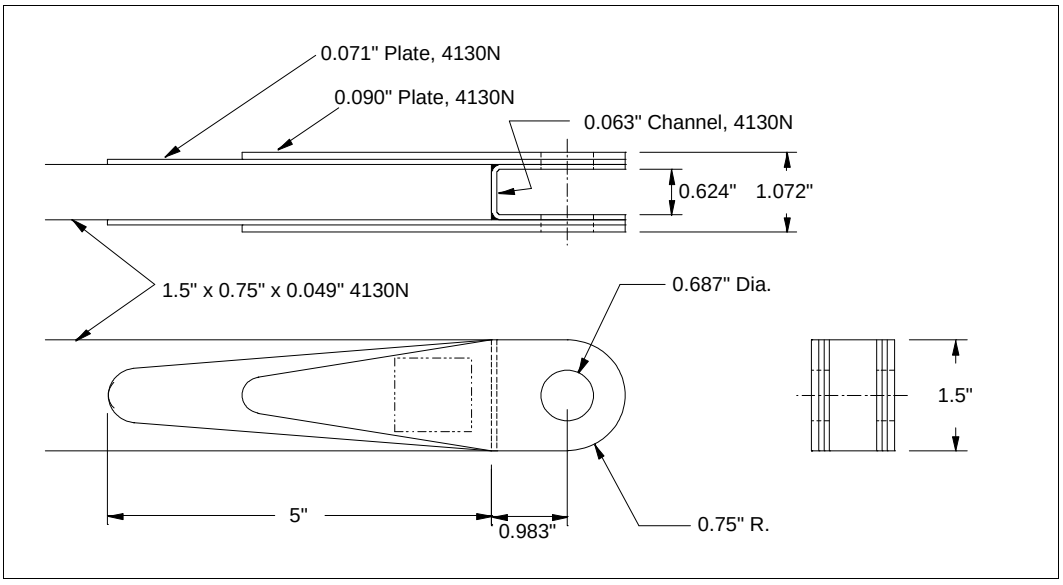

Figure 29. Fuselage Attachment Fitting, Aft Wing Spar.

strut attachment fittings. The wing rear spar attachment fitting is shown to use the same simple construction as the wing main spar fitting with laminated flat plates welded to the side of the rectangular tubing. The number of laminations was determined according to the allowable bearing stress on the attachment hole, the diameter of which was determined previously during the wing structural design. The fittings were checked for axial, bending shear stresses. Finally, the length of the fitting was determined according to the allowable shear stress in the weld itself.

Because of the vertical component of the wing and strut reactions, the attachment welds are eccentrically loaded with respect to the weld center of gravity. The total weld shear stress has been determined using [14]:

$$\tau_{weld} = \tau_{direct} + \tau_{moment}$$

where the direct component is:

$$\tau_{direct} = \frac{P}{0.7 \cdot t_{weld} \cdot l_{weld}}$$

and the moment contribution is:

$$\tau_{moment} = \frac{P \cdot e \cdot r}{J}$$

where:

e = eccentricity of the load

r = distance of the weld from the fitting cg.

$$J = \{0.7 \cdot t_{weld} \cdot l_{weld}\} \cdot \left\{\frac{l_{weld}^{2}}{12} + \bar{r}^{2}\right\}$$

$\bar{r}$ = distance from weld cg to the fitting cg.

In order to simplify the calculations, the weld has been conservatively approximated as shown in Figure 30. Note that the maximum weld stress shear stress occurs at the point farthest from the weld center of gravity. Table 16 summarizes the resulting stress levels for all three fittings.

6.4 Wing Strut

The proposed wing will utilize streamlined strut material readily available as surplus from the Cessna 100 series aircraft. A fitting will be installed at each end of the strut tube to mate with either the wing or fuselage fitting. By design the end fittings are identical. A cross section of the strut is shown in Figure 31 Since the strut is a one-dimensional member, the design challenges are limited, but the relatively thin wall of the streamlined tube requires a relatively large composite fastener diameter to keep the bearing stresses acceptable. The use of doublers was considered as a possibility, but the curvature of the streamlined cross section makes the manufacturing more complicated. Instead, the fitting was designed to be attached directly to the unmodified strut wall.

A sketch of the strut end fitting is shown in Figure 32 A fastener diameter of 0.25” was selected to accommodate the use of either AD rivets or AN bolts. Larger diameter fasteners would obviously reduce the number required and the associated length of the fitting, but rivet diameters larger than 0.25” are more difficult to set without special tooling. Considering the fitting in a bouble-shear condition, the resulting bearing stress in the hole of the strut wall is:

$$\sigma_{b_{fastener}} = \frac{8913 \text{ lbf}}{28\{0.25 \text{ in}\}\{0.1 \text{ in}\}} = 12.7 \text{ ksi}$$

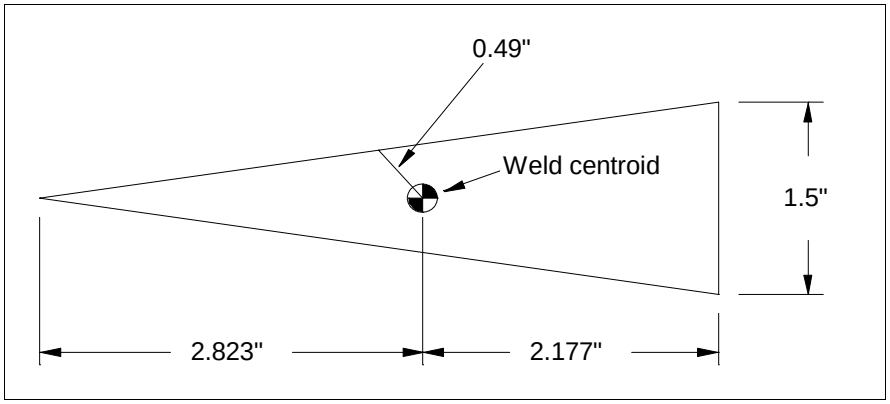

Figure 30. Fitting Weld Approximation.

Table 16. Summary of Fuselage Fitting Stresses (ksi).

	Wing (fwd)	Wing (aft)	Strut
$\sigma_{bearing_{hole}}$	24.8	15.2	20.1
$\sigma_{axial_{root}}$	10.2	6.8	7.0
$\sigma_{bending_{root}}$	6.5	7.1	17.0
τ_{root}	0.2	2.1	5.2
$\sigma_{max_{root}}$	16.8	14.1	24.8
$\tau_{tear-out_{hole}}$	NA	21.6	12.2
$\tau_{weld_{direct}}$	7.2	3.0	6.0
$\tau_{weld_{torsion}}$	3.9	2.9	11.9
τ_{weld}	8.7	4.8	16.3

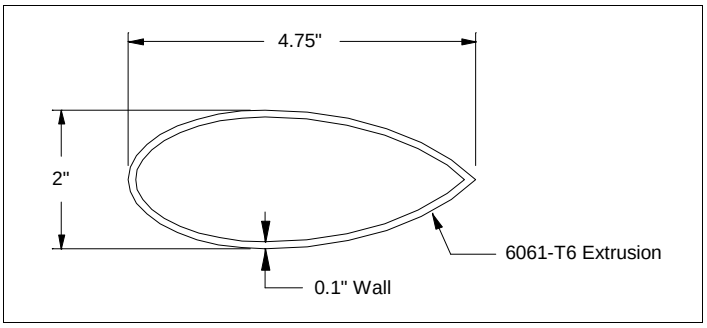

Figure 31. Streamlined Strut Cross Section.

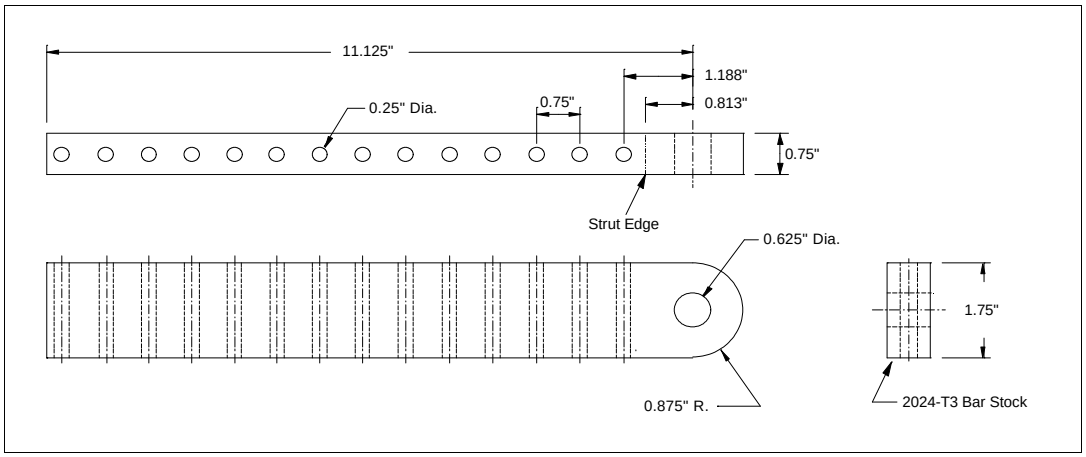

Figure 32. Strut End Fitting.

and the shear stress in the fastener is:

$$\tau_{fastener} = \frac{8913 \text{ lbf}}{28\left\{\frac{\pi}{4}\right\}\{0.25 \text{ in}\}^2} = 6.5 \text{ ksi}$$

One side of the strut tube could be countersunk for better streamlining. The use of rivets would result in a lower profile, but the bolts would be easier to install.

7. CONCLUSIONS AND RECOMMENDATIONS

7.1 Conclusions

A strut-braced, high-wing, 3 to 4-passenger airplane configuration was developed by utilizing the existing outer wing panels of the Mustang II kit airplane. The proposed airplane is expected to accommodate a 600 lb payload of up to 4 passengers at a cruise speed of 150 kts or greater in the Utility category by utilizing an off-the-shelf aircraft engine of nominally 230 hp. Independent strut-braced inboard wing sections were designed to utilize a simple primary structure of laminated aluminum spar cap strips. The simple but efficient steel tube cabin design helps to ensure that the proposed airplane configuration is suitable for construction by an amateur builder without the need for complex factory fixtures and tooling.

7.2 Recommendations

Further design effort is obviously necessary prior to any attempt at building the proposed airplane. Significant areas not addressed include the structural validation of the suitability of the RV-9 tail, as well as tail cone, and landing gear structural design. Note that a number of vendors experienced in landing gear design and manufacturing already support the amateur-built aircraft community with free design consultation. With these outstanding issues resolved, the proposed airplane design should be ready for construction by an experienced builder.

REFERENCES AND BIBLIOGRAPHY

REFERENCES

1. Federal Aviation Regulations Part 21, Volume II, Certification Procedures for Products and Parts, Washington: Department of Transportation, 1973.

2. http://www.aopa.org/whatsnew/newsitems/2002/02-3-086x.html

3. McCormick, Barnes W., Aerodynamic, Aeronautics, and Flight Mechanics, John Wiley & Sons, New York, 1979.

4. Bushby, R. W, "Bushby Mustang II Construction Drawings," Mustang Aeronautics Inc, Troy, MI, 1967.

5. Janes All the Worlds Aircraft, McGraw-Hill Book Co., 1962, 1971

6. Anonymous, "RV-9 Preview Construction Drawings," Vans Aircraft Inc., Aurora, OR, 2000.

7. Perkins, Courtland and Hage, Robert, Airplane Performance, Stability, and Control, Wiley and Sons, 1949.

8. Pazmany, Ladislao, Landing Gear Design for Light Aircraft, Volume 1, Pazmany Aircraft Corporation, San Diego, CA, 1986

9. Federal Aviation Regulations Part 23, Airworthiness Standards: Normal, Utility, and Acrobatic Category Airplanes, Washington: Department of Transportation, 1973.

10. Abbott, Ira H, and Von Doenhoff, Albert E., Theory of Wing Sections, Dover Publications, Inc., NY, 1959

11. Anonymous, The Cessna 170, Third Edition, The International Cessna 170 Association, Inc., Lebanon, MO, 1984.

12. Bruhn, E. F., Analysis and Design of Airplanes Structures, Tri-State Offset Co., Cincinnati, OH, 1949

13. Peery, David, J., Aircraft Structures, McGraw-Hill, New York, 1950.

14. Spotts, M. F., Design of Machine Elements, Prentice-Hall, Englewood Cliffs, NJ, 1985.

BIBLIOGRAPHY

1. Barrows, R., “Bearhawk Construction Drawings,” R & B Aircraft Co., Fincastle, VA, 1995.

2. Bede, James R., Build Your Own Airplane, Follett Publishing Co., Chicago, IL, 1977

3. Basic Glider Criteria Handbook, Federal Aviation Agency, Washington, D.C., 1962.

4. Guide to the Preparation of Theses and Dissertations, Eighth Edition, The Graduate School of the University of Tennessee, Knoxville, 2000.

5. Cessna 170B Parts Catalog, Cessna Aircraft Co., 1956

6. Mathcad User's Guide 2000, MathSoft, Inc., Cambridge, MA, 1999.

7. DesignCad 3D Max Version 12.0 Reference Manual, Upperspace Corp., Pryor, OK, 2001

8. StarOffice 6.0 User's Guide, Sun Microsystems, Inc. Palo Alto, CA, 2002.

VITA

David Andrew Moore was born in Greensboro NC on August 30, 1960. The family relocated first to Nashville, TN and later to near Chattanooga, TN where he attended The McCallie School for three years and graduated in 1978. His senior high school year included a fateful trip to the Chilhowee Gliderport in Benton TN where he soled a Schweizer 2-33A sailplane on January 2, 1978 after 12 instructional flights over 14 days. Learning to fly sailplanes, and towplanes, and then teaching others to fly sailplanes at the Chilhowee Gliderport fueled an enduring interest in aviation, airplane design and construction.

The University of Tennessee at Knoxville offered an Aerospace engineering program only an hours drive from the Chilhowee Gliderport, and after some years of study awarded him a Bachelor of Science Degree in May of 1983. One highlight during his undergraduate studies was the building (with quite a bit of help) and flying of the popular Schreder HP-18 sailplane.

An active and friendly flight research department combined with a first rate soaring club at the University of Tennessee Space Institute attracted him to start pursuing a graduate degree there in August 1983. In August 1984, after completing a year of full-time studies in Aerospace Engineering as a Graduate Research Assistant, he sought employment at the nearby Arnold Engineering and Development Center, where he continues to work as a Technical Engineering Specialist. And after a prolonged effort he finally received his Master's Degree in Mechanical Engineering in August 2003.